Elastic Scattering of Alpha Particles*

D. D. KERLEE,† J. S. BLAIR, AND G. W. FARWELL
Department of Physics, University of Washington, Seattle, Washington
(Received May 20, 1957)

An extensive study of elastic scattering of medium-energy alpha particles at fixed angles has been made for 28 nuclides ranging from Ni to Pu. The sharp-cutoff model is used to evaluate interaction radii, $R_{A\alpha}$, and a simple graphical method has been developed for these evaluations. A least squares fit to the experimental data of the form $R_{A\alpha}=r_0A^{\frac{1}{3}}+b$ gives $r_0=(1.414\pm0.042)\times10^{-13}$ cm, $b=(2.19\pm0.20)\times10^{-13}$ cm. The internal consistency of the data is much higher than the stated over-all errors (standard deviations) indicate; the average departure from the least squares curve is 0.75%. The dependence of interaction radius upon scattering angle is slight over the range of angles studied. Significant differences in interaction radius are seen between Pb and Bi and between U^{235} and U^{238}, among others. Small changes in either neutron or proton configuration influence the detailed structure of the curves of cross section *versus* energy, especially in the region of a closed neutron or proton shell. The angular and energy dependence of the structure in cross section curves is qualitatively discussed in terms of the sharp-cutoff model. A modification of this theory is used to estimate the cross section for an ellipsoidally distorted nucleus.

I. INTRODUCTION

ANOMALIES in the elastic scattering of alpha particles by Au, Ag, Ta, Pb, and Th were reported in 1954 by Farwell and Wegner.[1,2] Investigation of elastic scattering cross section *vs* energy in the region of 14 to 43 Mev showed that, for a particular element and scattering angle, the Rutherford energy dependence was followed as the alpha-particle energy was increased from 14 Mev up to a certain energy; at higher energies, a rapid and approximately exponential decrease in cross section was observed up to the maximum energy available. The energy at which departure from the Rutherford dependence begins was seen to increase with Z for the target element.

A semiclassical strong absorption model (hereafter termed the sharp-cutoff model) was used by Blair[3] to account for the general behavior of elastic scattering cross section as a function of energy over a considerable energy interval. In this model the outgoing lth partial wave vanishes if the corresponding classical turning point is less than the sum of the radii of alpha particle and nucleus (both radii are assumed to be sharply defined); otherwise it has a phase characteristic of pure Coulomb scattering. This model established a "quarter-point recipe" for evaluating the interaction distance $D_{1/4}$ (loosely, the sum of the radii) from the experimental curves; the data of Farwell and Wegner could be represented quite well by $D_{1/4}=r_0A^{\frac{1}{3}}+R_\alpha$, with $r_0=1.35$ to 1.5×10^{-13} cm and $R_\alpha=2.2$ to 1.4×10^{-13} cm.

Other authors[4–10] have subsequently published data on angular distributions of alpha particles scattered elastically by these elements, and others, at several different energies. Their data have been compared variously with the predictions of the sharp cutoff model, modifications of the sharp cutoff model which soften the transition from Coulomb scattering to complete absorption, and more sophisticated treatments such as the optical model. Further discussion of such interpretations will be given below in Sec. V.

The present series of experiments has extended over a period of several years. A number of questions raised by the earlier experiments have been answered, and a wide range of elements has been covered. Particular attention has been given to the following areas:

1. Technical changes[11] have resulted in great improvement in ease, accuracy, and consistency in taking data. This makes possible more accurate estimates of nuclear radii and clarifies some points in doubt in the earlier results; specifically, the rise in cross section just before the rapid falloff (see typical curves in Sec. III) has been found to be real and to vary markedly from one nuclide to another.

2. A continuous range of laboratory angles from 18° to 162° has been made available. Most of the early data were taken at 60°. It was thought important to establish the consistency with respect to scattering angle of nuclear radius determinations in terms of the sharp-cutoff model if the model were to be relied upon to provide useful information. A more general "crossover-point" criterion, which reduces approximately to the "quarter-point recipe" for scattering at 90°, has been developed (Sec. IV). A high degree of consistency has been established for nuclear radius determinations at different angles in terms of this criterion: for a given element for scattering angles of 42° and 60°, for example, a difference in radius of more than 1% is exceptional (Sec. IV).

3. In order to investigate both general trends with Z

* This work has been supported in part by the U. S. Atomic Energy Commission.
† Now at Seattle Pacific College, Seattle, Washington.
[1] G. W. Farwell and H. E. Wegner, Phys. Rev. **93**, 356 (1954).
[2] G. W. Farwell and H. E. Wegner, Phys. Rev. **95**, 1212 (1954).
[3] J. S. Blair, Phys. Rev. **95**, 1218 (1954).
[4] Wall, Rees, and Ford, Phys. Rev. **97**, 726 (1955).
[5] Wegner, Eisberg, and Igo, Phys. Rev. **99**, 825 (1955).
[6] L. Schechter and R. Ellis, Phys. Rev. **99**, 1044 (1955); **101**, 636 (1956).
[7] H. E. Gove, Phys. Rev. **99**, 1353 (1955).
[8] E. Bleuler and D. J. Tendam, Phys. Rev. **99**, 1605 (1955).
[9] Eisberg, Igo, and Wegner, Phys. Rev. **99**, 1606 (1955).
[10] Igo, Wegner, and Eisberg, Phys. Rev. **101**, 1508 (1956).
[11] These changes and other improvements are discussed more fully elsewhere: D. D. Kerlee, thesis, University of Washington, 1956 (unpublished).

and A and outstanding deviations from the general trends, 28 elements or individual nuclides ranging from Al to Pu have been studied. The interaction radii $R_{A\alpha}$ determined from the crossover-point criterion follow very closely a dependence upon A given by $R_{A\alpha}=r_0A^{\frac{1}{3}}+b$, with $r_0=(1.414\pm0.042)\times10^{-13}$ cm and $b=(2.19\pm0.20)\times10^{-13}$ cm (Sec. IV). There are exceptional cases, some of which are apparently correlated with nuclear shell closures. Trends in the cross-section curve structures are seen, and the effects of slight changes in nucleonic configuration are very noticeable in a few cases, especially near shell closures (Sec. V).

4. The sharp-cutoff model has been found to provide a qualitative understanding of the fine structure of the cross section *vs* energy curves of the present experiments as well as of the angular distributions taken at fixed energy (Sec. V).

II. APPARATUS AND EXPERIMENTAL PROCEDURE

The main features of the experimental procedure have been described in a previous paper.[2] 44-Mev alpha particles from the University of Washington 60-inch cyclotron were incident upon the target system. Thin copper degrader foils reduced the energy of the incident beam in finite steps covering a range of from 44 to 12 Mev. A two-unit proportional-counter telescope mounted on a scattering port detected the scattered particles; at each energy the differential range spectrum of the scattered particles was measured by this apparatus. The number of scattered particles observed was normalized to the charge collected by a Faraday cup behind the target.

Major changes[11] were made in the location of the scattering area and in the proportional-counter telescope.

Uncertainty in scattering angle caused by the fringing field of the cyclotron magnet, a troublesome feature of the earlier experiments, was eliminated by relocation of the scattering apparatus. A double-focusing uniform-field magnetic wedge focused the beam on the target assembly, which was mounted about 20 feet from the cyclotron in the center of the duct which carried the external beam. The scattering port built for use in the new location consisted of a truncated cylindrical turret mounted on a ball-bearing-supported vacuum seal in the beam duct. The turret was capped with a circular plate, also on a ball-bearing-supported vacuum seal. The sliding vacuum seals made it possible to change the scattering angle while the beam duct was under vacuum. The angle of truncation of the cylindrical turret was such that the solid angle presented to the proportional-counter telescope by the target remained constant at all angles of observation. A continuous range of scattering angles from 18° to 162° was available.

The degrader system was similar to the one used by Farwell and Wegner. At a particular scattering angle, the energy of the beam incident upon the target was selected by the copper-foil degrader system. Scattered particles passed through a beryllium-copper window, a foil-wheel absorber unit, and a short air space, and into the detector unit of the proportional-counter telescope.

The detector unit consisted of two thin proportional counters sharing a common envelope. A mixture of 4% CO_2 and 96% A filled the counters to an absolute pressure of 60 cm of Hg. Each counter was composed of 19 counter units in parallel. These counter units, similar to those described by Eisberg and Wegner,[12] consisted of hexagonal arrays of grounded 2-mil wolfram cathode wires centered around anode wires of the same dimensions and material. The anodes were operated at a potential of 1200 v. The counters proved extremely stable over a period of as much as one year of intermittent operation.

Signals from each of the two counters were amplified by shielded preamplifiers at the scattering area and linear amplifiers in a remote counting room. The linear amplifier outputs were fed into single-channel differential discriminator circuits; output pulses from the latter were fed into a coincidence circuit and scaler. The differential discriminator bias levels in the two channels were set to accept only pulses representing alpha particles whose specific ionization had reached a maximum in the second counter; thus a coincidence was recorded only when an alpha particle stopped in the second counter. Discrimination against protons was complete. The counter system was not sensitive to the high neutron and x-ray fluxes in the cyclotron room.

For a given scattering angle and degrader configuration, an abbreviated differential range curve taken with this apparatus yielded (a) the range of the elastically scattered alphas, which could be readily converted to energy, and (b) the relative counting rate, which could be converted to relative cross section. In an experimental run, the scattering angle was held fixed while the energy was varied in steps of about 1 Mev.

The full width at half-maximum of the elastic peak at 43.5 Mev was measured to be 1.6% in energy in a typical case. This represents substantial improvement in resolution over the earlier work.

Counting rates were normalized against integrated beam current. Current from the Faraday cup was allowed to charge a "fast" polystyrene capacitor of known value; the potential across the capacitor was measured with a quadrant electrometer. Electrometer readings were reproducible to within 1%. Two permanent magnets, producing a field of approximately 400 gauss when placed on either side of the copper Faraday cup, were used to prevent secondary electrons from escaping from the cup. It was found that with the magnets in place detectable secondary-emission leakage from the cup was absent in a region of from -300 v to $+300$ v cup voltage. The potential allowed to build up on the cup during a count did not normally exceed 2.5 v.

[12] R. M. Eisberg and H. E. Wegner, Rev. Sci. Instr. **25**, 1129 (1954).

Whenever available, self-supporting metal foil targets were used. Thin films of Sb and Bi metal were evaporated onto polystyrene sheets which were subsequently dissolved away, leaving self-supporting films of Sb and Bi. The rare earth materials, however, were available only in oxide and oxalate forms. These compounds were suspended in polystyrene films using a technique suggested by Wall and Irvine.[13] U (separated isotopes U^{235} and U^{238}), Np, and Pu targets were available as thin oxide films on aluminum foil.[14] Separated Pb isotopes were prepared as oxide (Pb^{206},Pb^{208}) and chromate (Pb^{207}) compounds in a plastic film.

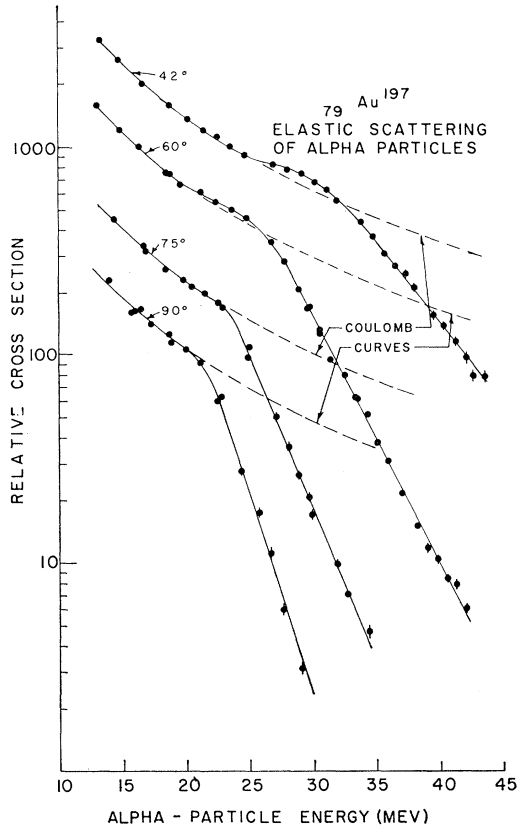

FIG. 1. Cross section *versus* energy for elastic scattering of alpha particles from $_{79}Au^{197}$ at laboratory angles of 42°, 60°, 75°, and 90°. Cross sections are plotted in arbitrary units; each experimental curve is normalized to a "Coulomb curve" representing the $1/E^2$ dependence of cross section upon energy (at fixed angle) given by the Rutherford formula. Alpha-particle energy means laboratory energy after scattering. In this and succeeding similar figures, the relative vertical positions of the curves displayed are chosen purely for convenience in plotting and thus have no numerical significance.

[13] N. S. Wall and J. W. Irvine, Jr., Rev. Sci. Instr. 24, 1146 (1953).

[14] We are indebted to Dr. Jane Hall of the Los Alamos Scientific Laboratory and Mr. K. E. Englund of the Hanford Operations Office of the U. S. Atomic Energy Commission for supplying these materials.

III. DATA

The energy dependence of alpha-particle elastic scattering cross sections for Ni, Cu, Zn, Ag, Sn, Sb, Ba, La, Ce, Pr, Sm, Eu, Tb, Er, Lu, Ta, Pt, Au, Pb, Bi, Th, U, Np, and Pu was studied. A "background run" on elastic scattering from 0.001-inch aluminum foil was also made, since some of the targets were on aluminum backings. We now present the data for the individual runs on all targets observed to date. Curves for Au and Pb are given first, since the wide range of angles at which data were taken for these elements provides a good picture of the trends observed for the heavy elements. Following this, we present data for other elements in order of atomic number and in groups which are convenient or especially illustrative.

$_{79}Au^{197}$, $_{82}Pb$.—Figure 1 shows the experimental results for $_{79}Au^{197}$ for several different scattering angles. These curves are typical of the results found for nearly all heavy elements. For the larger scattering angles, the effects of the nuclear forces are felt at lower energies, as would be expected in view of the closer penetration of the alpha to the nucleus. At high energies the approximately exponential decrease of cross section is more rapid at the larger scattering angles. At the smaller scattering angles, a brief rise in cross section relative to the Coulomb (Rutherford) cross section precedes the

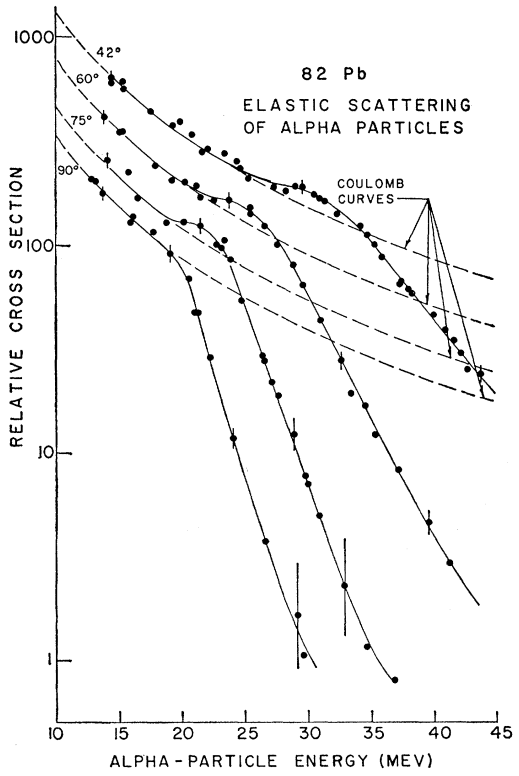

FIG. 2. Cross section *versus* energy for elastic scattering of alpha particles from $_{82}Pb$ (natural isotopic mixture) at laboratory angles of 42°, 60°, 75°, and 90°.

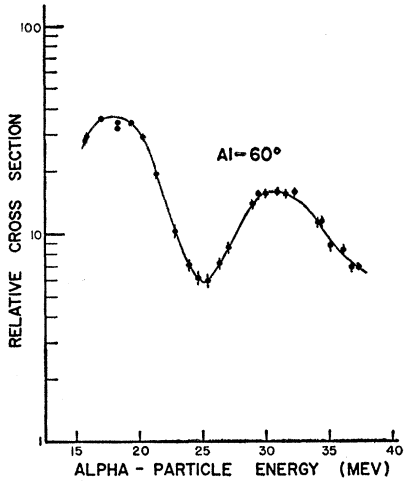

FIG. 3. Cross section *versus* energy for elastic scattering of alpha particles from $_{13}Al^{27}$ at 60° (lab).

downward break; this "rise," as we shall term it in the following discussion, is discernible in Au at 60° and is quite pronounced at 42°. All cross sections follow the Coulomb dependence well at low energies, affording an easy means of normalization. (The relative vertical positions of the curves of Fig. 1 and succeeding figures are chosen purely for convenience in plotting. Energies shown are for the alpha particles after scattering.)

A similar set of curves for $_{82}$Pb (natural isotopic mixture) is shown in Fig. 2. The rise is more pronounced here, and additional structure may be suggested; as will be seen below, these features are anomalously large in $_{82}Pb^{208}$.

A comparison of the Au and Pb curves shows that, for a given angle, the energy of downward departure from Coulomb is higher for Pb than for Au; this is, of course, a consequence of the fact that the nuclear charge has increased by a larger factor than has the nuclear radius.

$_{13}Al^{27}$.—The energy dependence of the elastic scattering from $_{13}Al^{27}$ was measured at 60° (Fig. 3). An oscillatory structure is observed, with peaks at 18 and 31 Mev and a minimum at 25 Mev. The average cross section drops by approximately a factor of three in the observed range of 16 to 37 Mev. No radius determination (Sec. IV) was attempted on Al, since the region of Coulomb scattering was not accessible.

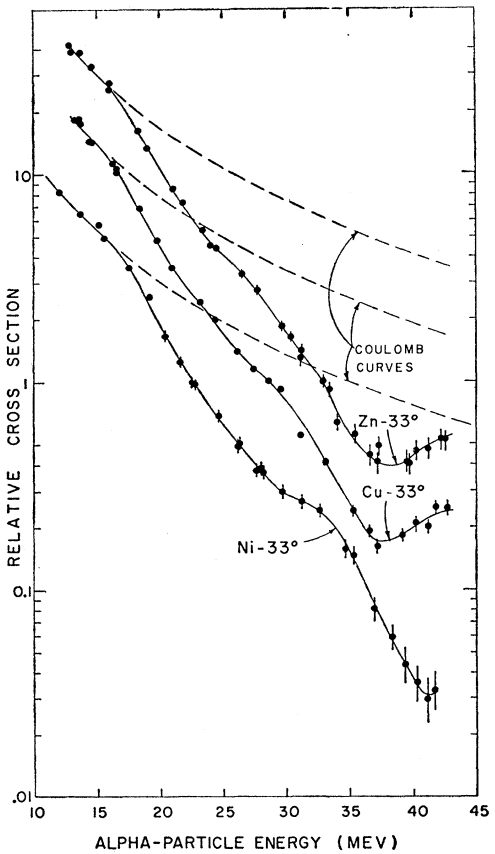

FIG. 4. Cross section *versus* energy for elastic scattering of alpha particles from $_{28}$Ni, $_{29}$Cu, and $_{30}$Zn at 33° (lab).

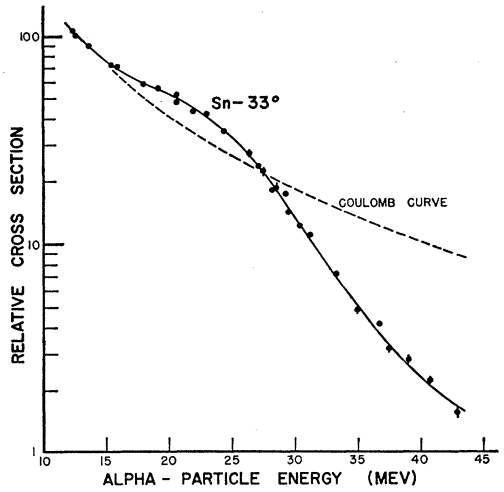

FIG. 5. Cross section *versus* energy for elastic scattering of alpha particles from $_{50}$Sn at 33° (lab).

Elements above Al*: general.*—Choice of angles of observation for the groups of elements listed below was made in accordance with two requirements. First, the angle must be small enough to provide a Coulomb scattering region of sufficient extent (in energy) to allow ready recognition and accurate normalization. Second, the angle must be large enough to give a region of rapid falloff in cross section to two-tenths Coulomb or less in order to make accurate estimate of the interaction radius possible (Sec. IV). The laboratory angles used were "33°" (actually 32° 54′) for the lightest elements, "42°" (actually 41° 34′) and "60°" (60° 00′) for intermediate elements, and 60° for the heaviest elements.

In comparing curves of cross section *vs* energy for the various elements, one notes a suggestion of oscil-

latory behavior in the lightest elements; sharp differences between certain neighboring elements or isotopes, especially with respect to height and extent of the rise; and other less prominent differences. A more detailed discussion of the differences in curve structure and their significance will be given in Sec. V; we remark here only that a large rise is probably associated with the especially sharply defined nuclear boundary which one might expect for singly or doubly "magic" nuclei such as Sn ($Z=50$) and Pb^{208} ($Z=50$, $N=126$).

In the following list, mass numbers are given only for those target materials consisting entirely or almost entirely of a single isotope.

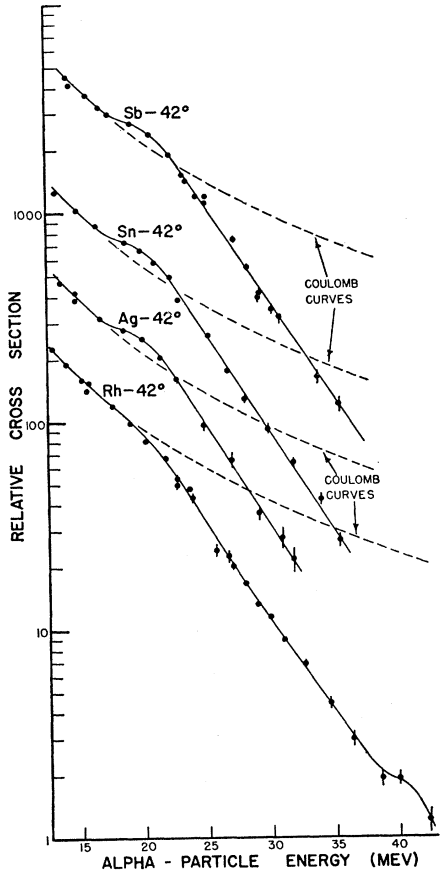

FIG. 6. Cross section *versus* energy for elastic scattering of alpha particles from $_{45}Rh^{103}$, $_{47}Ag$, $_{50}Sn$, and $_{51}Sb$ at 42° (lab).

$_{28}Ni$, $_{29}Cu$, $_{30}Zn$.—A transition between the exponential falloff observed for the heavy elements and the oscillatory pattern seen with aluminum is noticeable in the curves for $_{28}Ni$, $_{29}Cu$, and $_{30}Zn$ at 33° (Fig. 4). A nearly exponential behavior is observed in the 20-Mev region, but indications of a weak oscillatory behavior are present from approximately 25 to 35 Mev. Above 35 Mev a rise in the cross section is observed for Cu and Zn, indicating a possible oscillatory behavior similar to that of Al for energies beyond the reach of the experiment. For a few elements heavier than Zn, slight departures above the exponential falloff are also noticeable at the highest energies.

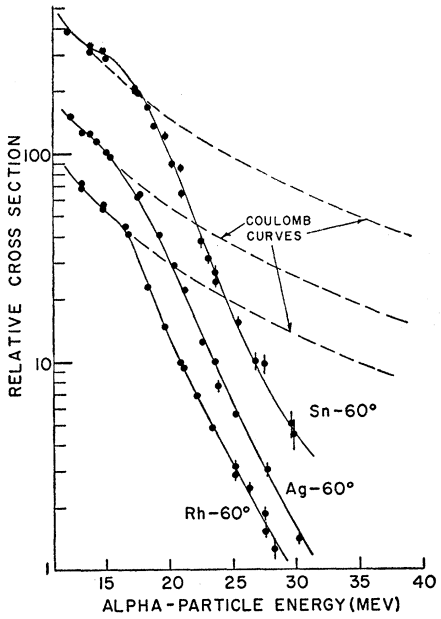

FIG. 7. Cross section *versus* energy for elastic scattering of alpha particles from $_{45}Rh^{103}$, $_{47}Ag$, and $_{50}Sn$ at 60° (lab).

$_{45}Rh^{103}$, $_{47}Ag$, $_{50}Sn$, $_{51}Sb$.—Curves are shown for Sn at 33° (Fig. 5); Rh, Ag, Sn, and Sb at 42° (Fig. 6); and Rh, Ag, and Sn at 60° (Fig. 7). Changes in the general curve features with scattering angle can be seen once more by comparing the data for Sn at 33°, 42°, and 60°.

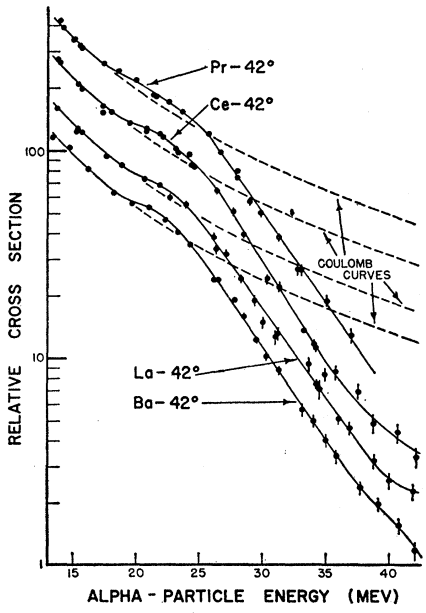

FIG. 8. Cross section *versus* energy for elastic scattering of alpha particles from $_{56}Ba$, $_{57}La^{139}$, $_{58}Ce$, and $_{59}Pr^{141}$ at 42° (lab).

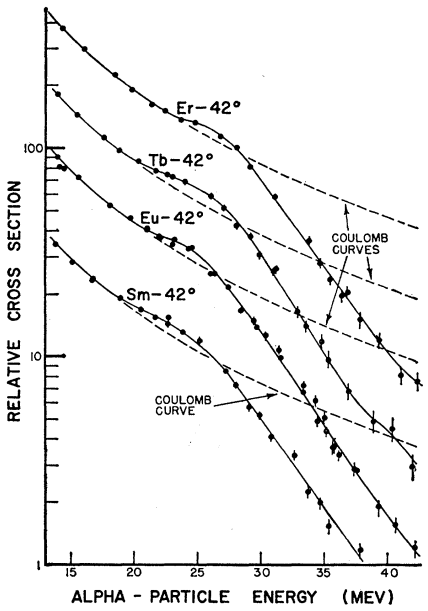

FIG. 9. Cross section *versus* energy for elastic scattering of alpha particles from $_{62}$Sm, $_{63}$Eu, $_{65}$Tb^{159}, and $_{68}$Er at 42° (lab).

At 33° the experimental cross section at the peak of the rise is 30% above the Coulomb cross section; smaller increases are noted at the larger angles. Above 36 Mev, a slowly increasing upward deviation from the initial exponential falloff is observed in the 33° curve; at the larger angles, this feature is much weaker or absent.

We observe a large difference between Rh (no rise) and Sn (largest rise) at both 42° and 60°.

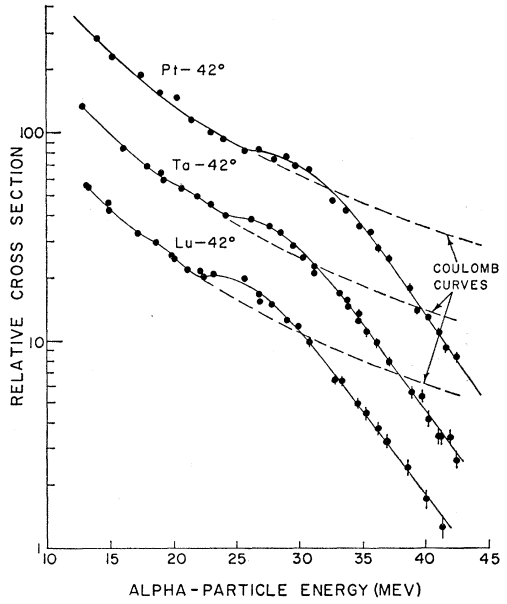

FIG. 10. Cross section *versus* energy for elastic scattering of alpha particles from $_{71}$Lu^{175}, $_{73}$Ta^{181}, and $_{78}$Pt at 42° (lab). For $_{79}$Au^{197} see Fig. 1.

$_{56}$Ba, $_{57}$La^{139}, $_{58}$Ce, $_{59}$Pr^{141}.—This is a series of targets progressing by steps of one in Z while N for all principal isotopes remains fixed at 82. Curves are given for 42° only (Fig. 8).

$_{62}$Sm, $_{63}$Eu, $_{65}$Tb^{159}, $_{68}$Er.—42° (Fig. 9).

$_{71}$Lu^{175}, $_{73}$Ta^{181}, $_{78}$Pt.—42° (Fig. 10); 60° (Fig. 11; Lu not studied).

$_{79}$Au^{197}.—Refer to Fig. 1.

$_{82}$Pb^{206}, $_{82}$Pb^{207}, $_{82}$Pb^{208}, $_{83}$Bi^{209}.—Exceptionally large differences between these nuclides at both 42° (Fig. 12) and 60° (Fig. 13) are seen. We postpone discussion to Secs. IV and V.

$_{90}$Th^{232}, $_{92}$U^{235}, $_{92}$U^{238}, $_{93}$Np^{237}, $_{94}$Pu^{239}.—60° (Fig. 14). A distinction between the two uranium isotopes can be seen in the energy at which the cross section drops below the Coulomb curve: for U^{238} this break occurs at an energy approximately 3 Mev lower than for U^{235}. Further, U^{235} has a small rise while U^{238} has none (Sec. V).

IV. THEORY AND RESULTS[15]: NUCLEAR RADII

A. Sharp-Cutoff Model

The present results are interpreted in terms of the sharp-cutoff model,[3] which has been surprisingly success-

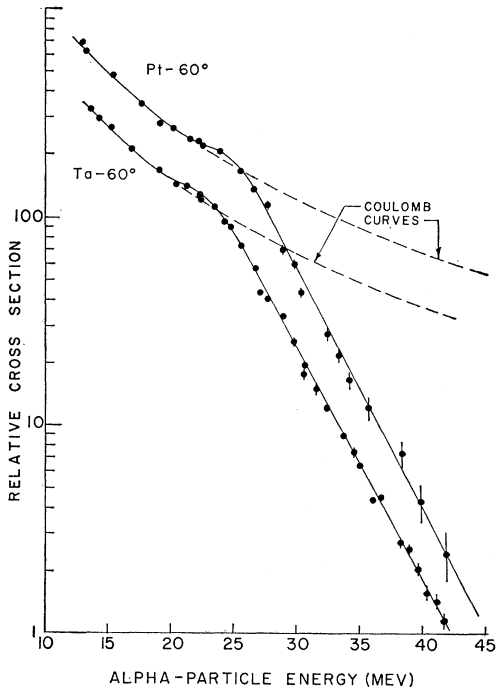

FIG. 11. Cross section *versus* energy for elastic scattering of alpha particles from $_{73}$Ta^{181} and $_{78}$Pt at 60° (lab). For $_{79}$Au^{197} see Fig. 1.

[15] Partial results have been reported from time to time: Kerlee, Blair, and Farwell, Phys. Rev. **99**, 1652 (A) (1955); G. W. Farwell, Bull. Am. Phys. Soc. Ser. II, **1**, 245 (1956); Progress Report, Cyclotron Research, University of Washington, 1956 (unpublished); see also reference 11; Farwell, Kerlee, Rickey, and Robison, Physica **22**, 1127 (1956).

ful in explaining many of the features of elastic scattering of alpha particles and other charged nuclear particles when the classical parameter $n \equiv ZZ'e^2/\hbar v$ is much larger than unity.[2–7,16] In brief, the main assumption of the model is that the strong absorption by the nucleus is represented by the following boundary condition on η_l, the coefficient of the outgoing lth partial wave[17,18]:

$$\begin{aligned} \eta_l &= 0 \quad \text{if} \quad l \leqq l', \\ \eta_l &= \exp(2i\sigma_l) \quad \text{if} \quad l > l', \end{aligned} \tag{1}$$

where σ_l is the readily calculated phase shift for pure Coulomb scattering and $\hbar l'$ is that angular momentum for which the particle can classically just overcome the potential barrier and penetrate to the interior of the nucleus. In the specific case of a nucleus described by an attractive absorbing well with a sharply defined radius R_n, $\hbar l'$ is accordingly that angular momentum for which the classical Coulomb turning point is equal to the sharp-cutoff radius, $R = R_n + R_\alpha$:

$$E = ZZ'e^2/R + \hbar^2 l'(l'+1)/2mR^2. \tag{2}$$

The model has the virtues that it is relatively easy to compute the theoretical cross sections and that there is but one free parameter, namely, l' or equivalently R. Thus to the extent to which the model reproduces the experimental behavior it furnishes an operationally defined "radius" for each nucleus investigated.

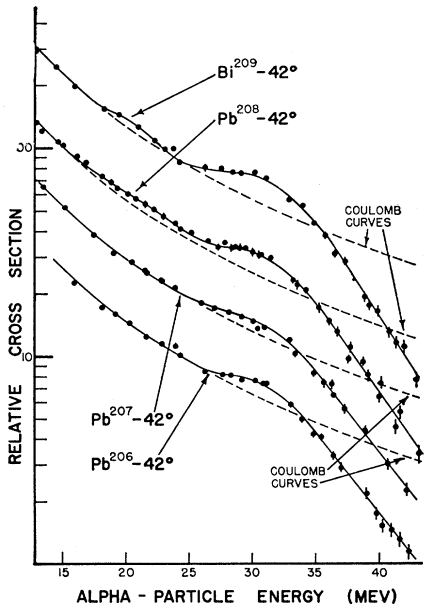

FIG. 12. Cross section *versus* energy for elastic scattering of alpha particles from $_{82}Pb^{206}$, $_{82}Pb^{207}$, $_{82}Pb^{208}$, and $_{83}Bi^{209}$ at 42° (lab). (See also Fig. 2.)

[16] H. L. Reynolds and A. Zucker, Phys. Rev. **102**, 1378 (1956).
[17] A. Akhieser and I. Pomeranchuk, J. Phys. (U.S.S.R.) **9**, 471 (1945).
[18] E. Clementel and A. Coen, Nuovo cimento **10**, 988 (1953).

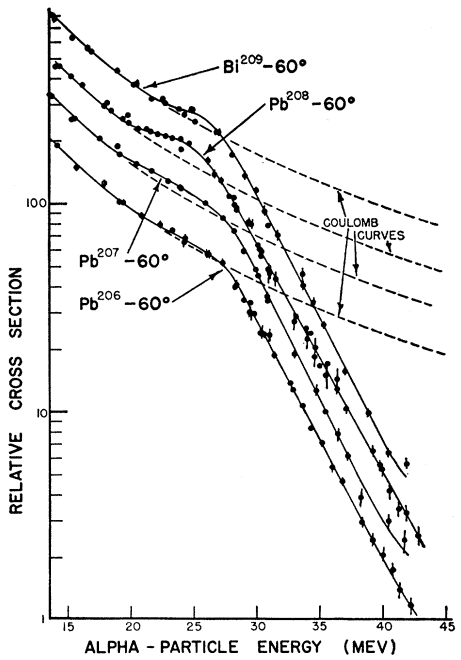

FIG. 13. Cross section *versus* energy for elastic scattering of alpha particles from $_{82}Pb^{206}$, $_{82}Pb^{207}$, $_{82}Pb^{208}$, and $_{83}Bi^{209}$ at 60° (lab). (See also Fig. 2.)

To indicate the suitability of the model, computed cross sections are compared with present experiments in Figs. 15 and 16. The experimental curves for cross section *vs* energy for alphas scattered at 60° by Pb^{207} and by Pb^{208} are indicated by solid lines, while the theoretical values of cross sections are given by the dots for three different values of R. (The scatter of experimental points about the solid curve can be seen in Fig. 13.) It is clear from Eqs. (1) and (2) that for a given R only a discrete number of energies correspond to integral values of l', and the theoretical points are computed for just these energies. The computational labors were greatly eased through use of the University of Washington IBM 604 electronic calculator, which, indeed, made it unnecessary to use the rough graphical interpolation methods of reference 3 in order to obtain plots of σ *vs* E.

The calculated cross sections exhibit the following features: (a) The general trend of the points shows a definite break below the pure Coulomb curve, the location of the break depending critically on the assumed radius; the average slope in the region encompassing approximately half a decade below Coulomb matches the experimental slope rather well for most elements examined. (b) Before the break there is a very pronounced rise above the pure Coulomb curve. Such a rise is observed for the majority of nuclei examined experimentally, and we believe it is intimately related to the condition of the nuclear surface.[19] (c) The

[19] Because of the variation in the rise with target material, we do not believe it is correct to place too much emphasis on the quality of the fit in the region of the rise in determining the best-fit radii.

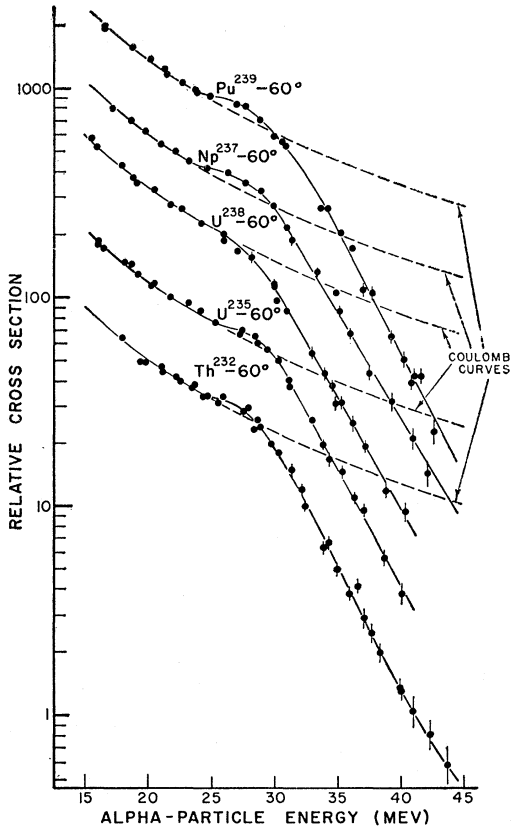

FIG. 14. Cross section *versus* energy for elastic scatter ng of alpha particles from $_{90}Th^{232}$, $_{92}U^{235}$, $_{92}U^{238}$, $_{93}Np^{237}$, and $_{94}Pu^{239}$ at 60° (lab).

computed points tend to level off after they have fallen about a decade below Coulomb; this failure of the model to match the continuing downward experimental curves is attributable to the assumed sharp transition in the amplitudes of the outgoing partial waves. (d) The nature of the scatter of the points for integral l' suggests that a sensible interpolation to nonintegral values of l' would produce a smooth curve displaying rapid oscillations about the general trend, which we shall term "diffraction oscillations." Indeed, corresponding oscillations in the angular distribution are found when the model is used to calculate the elastic cross section as a function of angle for fixed l' and E.[4–6] Such oscillations have not been seen in the present experiments except for targets of rather low Z, but the corresponding oscillations have been observed in angular distributions.[6,8–10] We believe that the reason these diffraction oscillations are not apparent in the present experiments is not that they are masked by lack of experimental resolution; rather, it is that almost any realistic improvement in the boundary conditions suffices to damp them out for the range of the parameters n and ϕ applicable to our experiments. Contrary to the implication of reference 3, we now believe that the computed oscillations will be present under certain conditions. We postpone further discussion of the reasons for these statements as well as additional comments on the fine structure until Sec. V. In what follows on the determination of sharp-cutoff radii from present experiments, we assume that it is reasonable to damp out the diffraction oscillations and consider the average behavior of σ.

Returning to Figs. 15 and 16, we see that for Pb^{207} the calculated points for $R=10.47\times10^{-13}$ cm straddle the experimental curve. In the case of Pb^{208}, the radius $R=10.67\times10^{-13}$ cm gives the best general fit to experiment in the range down to $\sim\frac{1}{5}$ pure Coulomb, although the points seem to lie slightly below the experimental curve. On the other hand, the calculated points for $R=10.47\times10^{-13}$ cm fall slightly above the experimental curve, while those for $R=10.27\times10^{-13}$ cm lie considerably above experiment. Since the computations are for ϕ (center-of-mass angle) $=60°$ while the experiment is performed at $\phi=60°\ 58'$, a small correction in

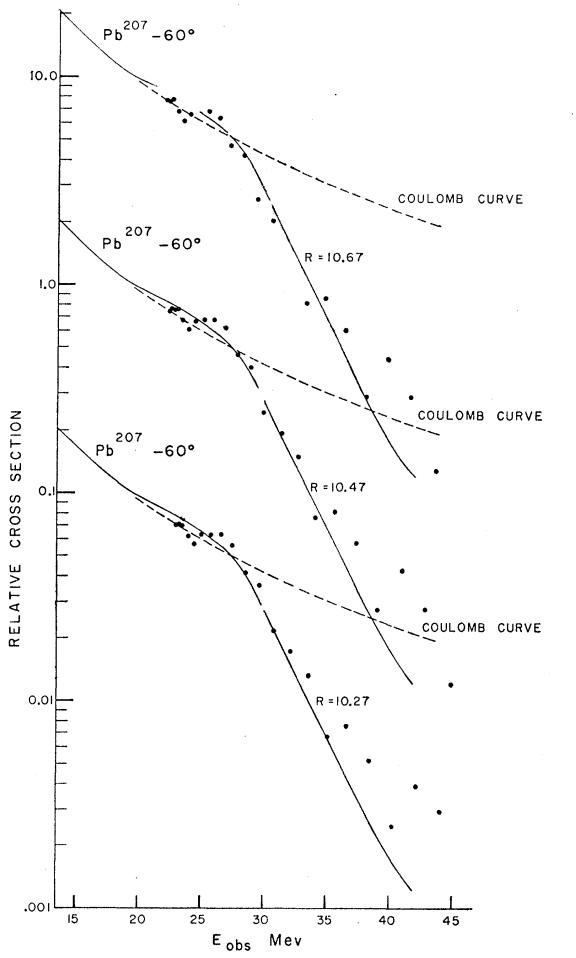

FIG. 15. Cross section *versus* energy for elastic scattering of alpha particles from $_{82}Pb^{207}$. The solid curves represent the experimental data for laboratory scattering angle $=60°$; the dots give the cross sections computed with the sharp-cutoff model for center-of-mass angle $=60°$, for three values of cutoff radius: 10.67, 10.47, and 10.27×10^{-13} cm.

radii is necessary. After correction we find that the radii giving the best general fit at $\phi=60°\,58'$ are $(10.4\pm0.2)\times10^{-13}$ cm for Pb^{207} and $(10.5\pm0.2)\times10^{-13}$ cm for Pb^{208}; the indicated errors are reflections of our visual uncertainty in assessing the best fits.

In principle we can find R for each target by determining in similar fashion the radius giving the best over-all fit in the region just below the break. In practice, such a procedure is quite time-consuming, so that it is advantageous to have a simpler method of radius determination. One such procedure is the one-quarter-point recipe,[3] whose merits and defects will be reviewed below in Sec. 1. This prescription is not accurate enough for analysis of the present data and has been replaced by the closely related crossover-point recipe discussed in Sec. 2.

1. One-Quarter-Point Recipe

When $G\equiv\sigma/\sigma_c$, the ratio of cross section to Coulomb cross section as calculated in the sharp-cutoff model, is plotted *versus* l'/n at $\phi=90°$ for various values of n, it is observed that all the curves joining the computed points cross at approximately $G=\frac{1}{4}$ for $\hbar l'=\hbar n\cot(90°/2)$, the classical angular momentum corresponding to scattering angle 90°. (See Fig. 1 of reference 3.) This leads to the simple prescription that R equals $D_{1/4}$, the classical distance of closest approach, evaluated at the energy for which $G=\frac{1}{4}$. One has a simple picture supporting the recipe: the Coulomb wave packet is centered about the classical trajectory so that, if the sum of the nuclear and alpha radii equals the classical distance of closest approach and if the nucleus is assumed opaque for alpha particles, then only half the amplitude of the packet remains; the scattered intensity is thus one-quarter of that observed for pure Coulomb scattering.

The one-quarter-point recipe has the virtues of simplicity in application, since it is independent of the parameter n, as well as simplicity in understanding. It is not accurate enough, however, to be used in precise determinations of the sharp-cutoff radii for the following reasons: (a) Close inspection shows that the curves of G *vs* n for the case $\phi=90°$ do not cross precisely at $l'=n$ but rather at $l'=0.94n$, with a corresponding value of $G=0.316$. Where $l'=n$, G ranges from ~0.277 for $n=7$ to ~0.264 for $n=10$.[20] (b) Even when l' does equal $n\cot(\phi/2)$, the corresponding R as given by Eq. (2) is slightly larger than D by an amount $(\lambda\!\!\!^{-}/2)\cos(\phi/2)$. This is a consequence of the usual shift of half a unit in angular momentum between the classical and quantum mechanical angular momenta. (c) When $\phi\neq90°$ there is the additional complication

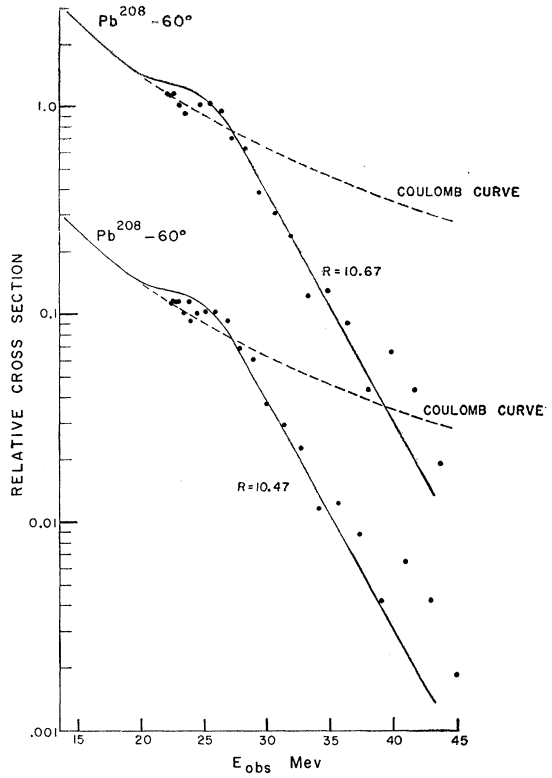

FIG. 16. Cross section *versus* energy for elastic scattering of alpha particles from $_{82}Pb^{208}$. The solid curves represent the experimental data for laboratory scattering angle=60°; the dots give the cross sections computed with the sharp-cutoff model for center-of-mass angle=60° for two values of cutoff radius: 10.67 and 10.47×10^{-13} cm.

that values of G for a given n cannot be joined by a smoothly decreasing curve. (See Fig. 3 of reference 3.) In the expectation that the rapid oscillations are damped out the oscillating curve is replaced by an average curve which bisects the envelope curves. Again it is found that such smoothed plots of G *vs* l'/n for various n do not have a common value, 0.25, at $l'=n\cot(\phi/2)$ but, instead, slightly higher values. Thus the radii determined from such smoothed plots will be larger than those given by the one-quarter-point recipe.

2. Crossover-Point Recipe

Although the averaged plots of the computed G *vs* l'/n do not cross where l' corresponds to the classical angular momentum, it is observed that they do form a small pencil at some smaller value of l'/n. Plots of average G have been constructed for 10 angles between 33° and 110°. n was varied from 5 to 12 in integral steps; in all cases there was a definite region of crossover. Figure 17 displays such a plot for $\phi=42°\,40.5'$. The fact that a common value of the ratio of the cross sections does exist is the basis of the "crossover-point" recipe.

[20] Figure 1 of reference 3 is slightly in error since the curves were drawn only through the points l_{even}'. The correct procedure at 90° is to pass the curves through the points $(l_{\text{even}}'+\frac{1}{2})$ as has been done by Wall, Rees, and Ford in Fig. 9 of reference 4; that this is correct is indicated by the fact that the location of the "crossover" is then the same as that obtained by interpolating results at neighboring angles.

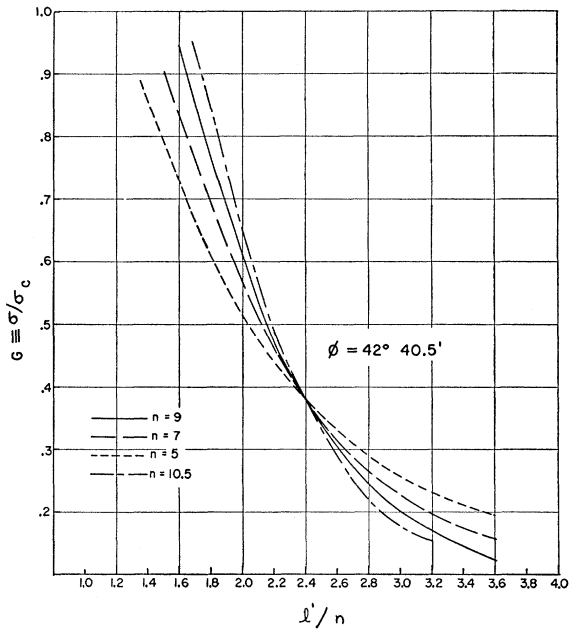

FIG. 17. The ratio, $\sigma/\sigma_c \equiv G$, averaged over rapid oscillations, plotted as a function of l'/n for several values of n when the center-of-mass angle is 42° 40.5′. Crossover occurs at $G=0.388$, $l'/n=2.365$.

The ratio of cross sections at crossover is a slowly varying function of scattering angle, as may be seen from Fig. 18. The quantity R/D_{cr}, the ratio of cutoff radius to classical distance of closest approach for the angle and energy at which crossover occurs, also varies slowly with angle. Plots of R/D_{cr} for typical n values are given in Fig. 19.

The crossover-point recipe is then: (a) Find the energy at which the experimental G for a given angle equals the crossover ratio as given by Fig. 18. (b) Compute D_{cr} for this angle and energy. (c) Determine R by using Fig. 19 to find the correct ratio R/D_{cr}; this latter ratio depends to a small extent upon n, which must be evaluated at the crossover energy.

There is an uncertainty conservatively estimated to be of order ± 0.015 in $(l'/n)_{cr}$ due to the graphical

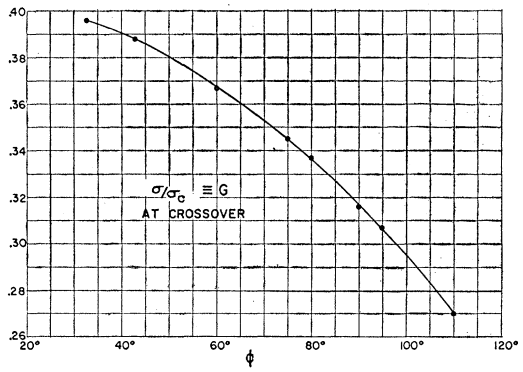

FIG. 18. G at crossover as a function of center-of-mass angle ϕ.

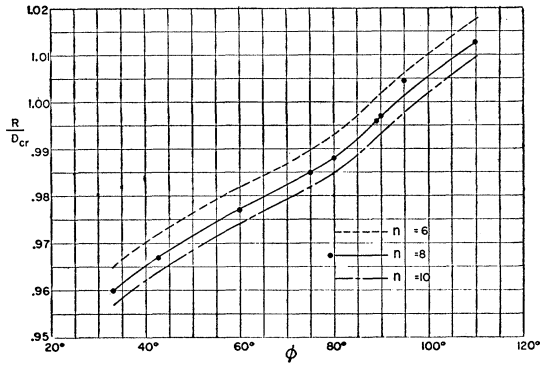

FIG. 19. R/D_{cr} as a function of center-of-mass angle ϕ for $n=10$, 8, and 6.

methods used in constructing these plots; such an error leads to an uncertainty of order $\pm 0.3\%$ in R.

If the crossover recipe with its enormous time-saving advantages is to be considered a trustworthy procedure, it should yield the same value of sharp-cutoff

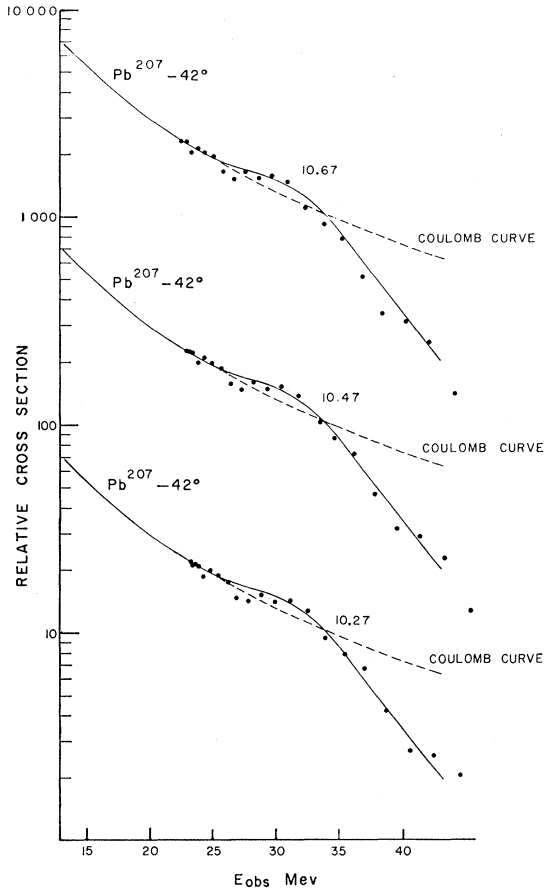

FIG. 20. Cross section *versus* energy for elastic scattering of alpha particles from $_{82}Pb^{207}$ at center-of-mass angle = 42° 18′. The solid curves represent the experimental data, while the dots give the cross sections computed with the sharp-cutoff model for three values of cutoff radius: 10.67, 10.47, and 10.27×10^{-13} cm.

radius as that obtained from the best over-all fit below the break. The best-fit radius for Pb^{207} at 60° was given in a previous paragraph as $(10.4\pm0.2)\times10^{-13}$ cm; this is in good agreement with the value 10.49 ± 0.07 (we use the same unit, 10^{-13} cm, hereafter) given below in Table I for the radius determined from the crossover-point recipe. For Pb^{208}, the corresponding figures are 10.5 ± 0.2 (best-fit radius) and 10.47 ± 0.04 (crossover radius).

We have also computed G *vs* E for scattering at 42° from the Pb isotopes. Figure 20 (Pb^{207}) indicates a best match to the experimental curve, with regard to both slope and amplitude, for $R=10.47$. This is to be compared with the crossover radius of 10.46 ± 0.04 (Table I). Figure 21 (Pb^{208}) presents the case of poorest agreement: the best-fit radius (10.27) is 0.2 below the crossover radius (10.48 ± 0.03). In this instance, where the nucleus is doubly magic, the experimental initial rise is higher and broader than that computed, and the observed slope following the break is distinctly larger than predicted. Since in a determination of best over-all fit all points following the break region are weighted equally, the best-fit radius is then slightly smaller than the crossover radius.

From these comparisons as well as from others not discussed here, we estimate the uncertainty in R due to application of the crossover criterion rather than best fit calculations to be approximately $\pm0.1\times10^{-13}$ cm; in exceptional cases where the initial rise is abnormally large, the uncertainty may be as much as $\pm0.2\times10^{-13}$ cm.

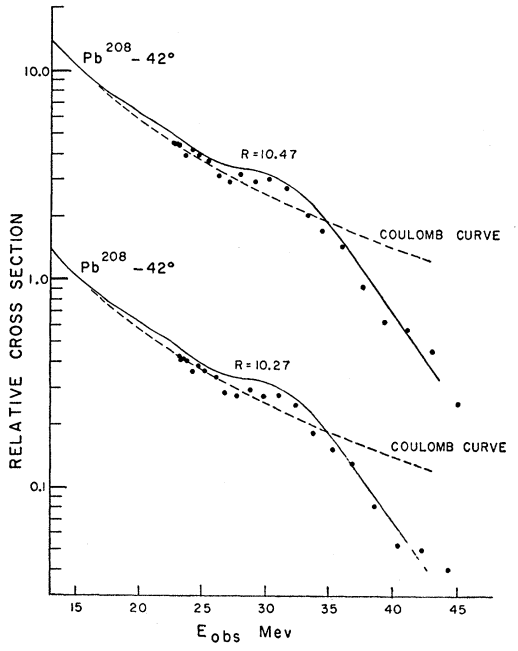

FIG. 21. Cross section *versus* energy for elastic scattering of alpha particles from $_{82}Pb^{208}$ at center-of-mass angle=42° 18′. The solid curves represent the experimental data, while the dots give the cross sections computed with the sharp-cutoff model for two values of cutoff radius: 10.47 and 10.27×10^{-13} cm.

B. Interaction Radii

We define the "interaction radius" $R_{A\alpha}$ for elastic scattering of alpha particles from a given nucleus as the sharp-cutoff radius determined by application of the crossover-point criterion to the experimental data.

1. Experimental Results

Table I summarizes the results obtained in the present experiments.

2. Errors

The errors given in Table I are standard deviations corresponding to what we shall call internal experimental errors, *viz.*, those due to the uncertainties in determination of E_{cr} from the experimental data. They are essentially curve-fitting errors, both in the Coulomb region where normalization is made and in the higher energy region beyond the break. They are usually $\pm1\%$ (about 0.1×10^{-13} cm) or less, although in a few cases they are larger. The small errors are a consequence of the fact that it is usually possible to locate E_{cr} with high precision. For example, for Au at 60° (Fig. 1) the Coulomb region is very well defined, and the slope in

TABLE I. Interaction radii $R_{A\alpha}$ for elastic scattering of alpha particles.

Target[a]				Interaction radius[b] $R_{A\alpha}$		
Z	Element	A	N	33°	42°	60°
28	Ni			7.66±0.13		
29	Cu		34	7.81±0.09		
30	Zn			7.86±0.10		
45	Rh	103	58		8.73±0.08	8.85±0.08
47	Ag				8.88±0.08	8.94±0.09
50	Sn			9.23±0.20	9.19±0.06	9.14±0.11
51	Sb				9.23±0.05	
56	Ba				9.47±0.05	
57	La	139	82		9.44±0.05	
58	Ce				9.67±0.07	
59	Pr	141	82		9.56±0.06	
62	Sm				9.67±0.07	
63	Eu				9.90±0.07	
65	Tb	159	94		9.98±0.05	
68	Er				10.07±0.08	
71	Lu	175	104		9.99±0.05	
73	Ta	181	108		10.00±0.04	10.26±0.14
78	Pt				10.33±0.08	10.43±0.14
79	Au	197	118		10.37±0.04	10.42±0.05
82	Pb	206	124		10.45±0.04	10.45±0.05
82	Pb	207	125		10.46±0.04	10.49±0.07
82	Pb	208	126		10.48±0.03	10.47±0.04
83	Bi	209	126		10.66±0.07	10.60±0.07
90	Th	232	142			11.02±0.12
92	U	235	143			10.90±0.05
92	U	238	146			11.30±0.06
93	Np	237	144			10.85±0.06
94	Pu	239	145			10.89±0.06

[a] A and N are listed only for those targets consisting entirely or almost entirely of a single isotope.
[b] Radii are expressed in units of 10^{-13} cm. Errors are standard deviations derived from estimated "internal" error in finding E_{cr} from the experimental data (see text).

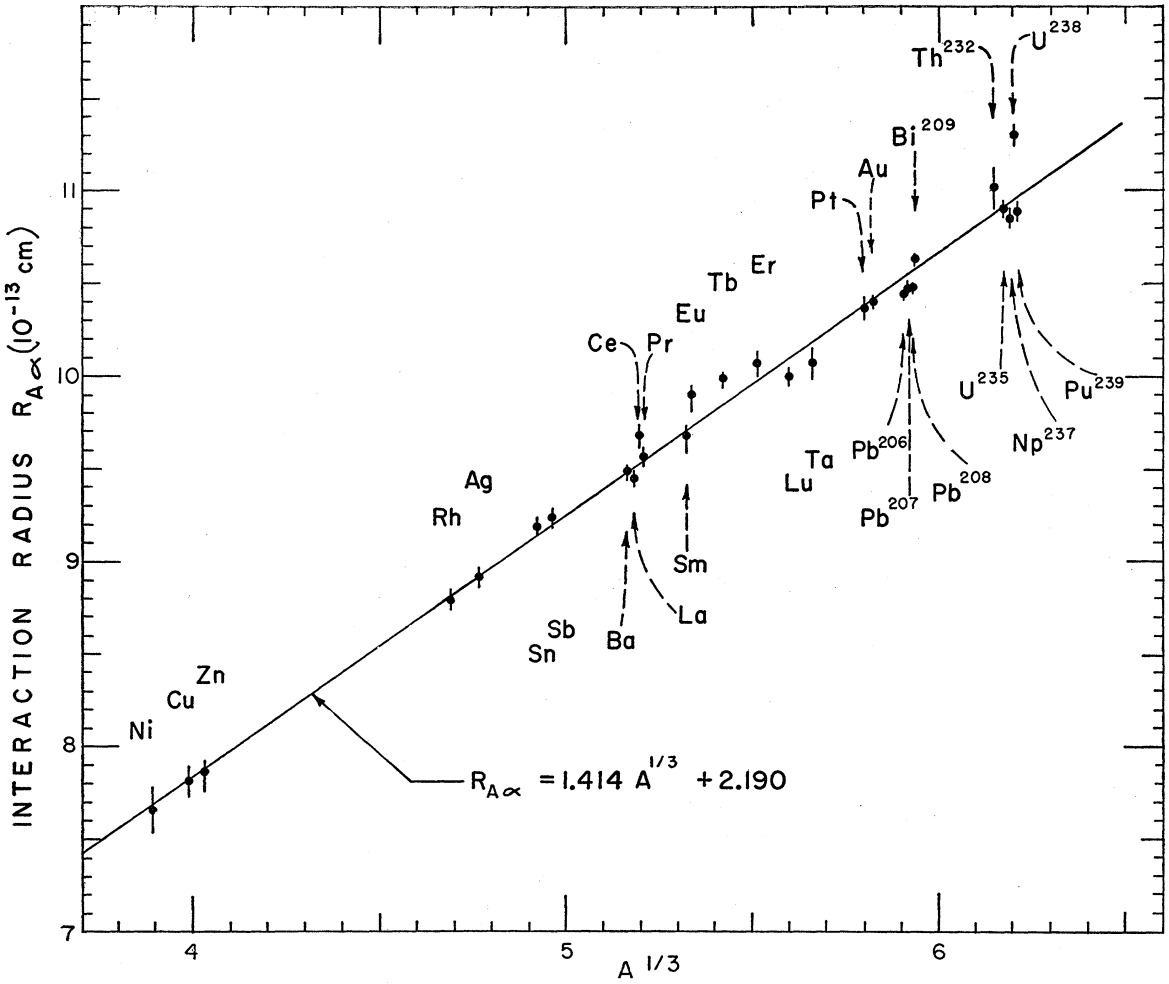

FIG. 22. $R_{A\alpha}$, the interaction radius for elastic scattering of alpha particles as determined from the crossover criterion of the sharp-cutoff model, is plotted against $A^{\frac{1}{3}}$. The value of $R_{A\alpha}$ for each target is a weighted average of the values given in Table I for different angles. Only internal experimental errors are shown. The solid line represents the least squares straight-line solution $R_{A\alpha}=(1.414A^{\frac{1}{3}}+2.19)\times10^{-13}$ cm.

the region of E_{cr} (31.7 Mev) is large: in an interval of 0.3 Mev (~1% in energy), σ/σ_c drops from 0.364 to 0.337. Since $R\propto 1/E_{cr}$, correspondingly high precision in R is achieved.

In estimating the absolute accuracy of the results, other sources of error must be considered. Internal theoretical errors—those associated with possible discrepancy between best-fit and crossover radii and those due to the graphical methods employed in Figs. 18 and 19—have already been estimated to be about ±1% (0.1×10^{-13} cm) in most cases. These errors vary from target to target. External experimental errors, however, affect all results in almost identical fashion. They consist of errors in scattering angle (less than 0.5°), errors in target and window thickness corrections, and errors in energy determinations from range data. We estimate the external experimental errors at ±1.5%. The combined uncertainties in absolute values of the individual interaction radii are then about ±2% (standard deviation), although the internal consistency of the numerical results is considerably better than this.

3. *Consistency with Respect to Angle*

Inspection of the data of Table I reveals a high degree of consistency of interaction radii with respect to angle—an important consideration in evaluating the usefulness of the sharp-cutoff model. Radii determined for the same element or nuclide from data taken at different angles agree within less than 0.1×10^{-13} cm in eight out of ten cases where comparisons can be made. Agreement within the assigned internal experimental errors is found for all cases except Ta, which shows a discrepancy of 0.26×10^{-13} cm between the results for 42° and 60°.

In order to test the consistency over a wider range of angles, the cross section of Au was studied at 75° and 90° (Fig. 1). The interaction radii for Au at 42°, 60°,

75°, and 90° are 10.37±0.04, 10.42±0.05, 10.57±0.08, and 10.65±0.09, respectively (units of 10^{-13} cm). Thus a small but distinguishable trend toward larger crossover radii with increasing angle, or alternatively with decreasing crossover energy, is indicated. A similar trend is found when the observed angular distributions are analyzed with the sharp-cutoff model.[4,21]

These trends can be qualitatively understood when the nuclear surface is not considered to be perfectly sharp but, rather, is represented by an exponentially decreasing attractive potential. It is then found that the sharp-cutoff radii, as determined by the crossover recipe, increase somewhat with increasing angle, a point which we develop elsewhere.[21] In view of the uncertainty in some of the assumptions in this analysis, however, and the observation[22] that the nuclear potential itself appears energy dependent, we refrain from attempting to correct the crossover radii here obtained for such an angular dependence. In the next section we assess the possible effect of such a trend upon the $A^{\frac{1}{3}}$ dependence of the observed interaction radii.

4. *Dependence upon A*

The weighted average of the measurements given in Table I for each target was taken to obtain a best value of $R_{A\alpha}$ for that target. The resulting interaction radii are plotted against $A^{\frac{1}{3}}$ in Fig. 22. Only internal experimental errors were considered in assigning errors to the plotted points.

A least squares solution of the form $R_{A\alpha}=r_0A^{\frac{1}{3}}+b$ was fitted to the data given in Table I. The solution yielded $r_0=1.414\pm0.036$ and $b=2.19\pm0.20$. (Units are 10^{-13} cm; errors are standard deviations from internal errors.) This least squares solution is also shown in Fig. 22 as the straight line

$$R_{A\alpha}=(1.414A^{\frac{1}{3}}+2.19)\times10^{-13}\text{ cm}. \quad (3)$$

If there should be an appreciable angular dependence of the crossover radii, the stated values of r_0 and b would be influenced, since the radii of the lighter nuclei are measured at smaller angles than are those of the heavier nuclei. On the basis of the small and somewhat uncertain trend observed experimentally (see also Table I for elements other than Au), we estimate that it might be necessary to lower r_0 by as much as 0.03×10^{-13} cm and to raise b by 0.2×10^{-13} cm.

The most striking feature of the over-all results is the close adherence of the interaction radii to the $A^{\frac{1}{3}}$ dependence. The average deviation from Eq. (3) is 0.75%; out of twenty-eight cases, one deviation is 3% (U^{238}), seven are between 1% and 2%, and twenty are less than 1%.

Deviations ($\Delta R_{A\alpha}$) from Eq. (3) are plotted against A in Fig. 23. No general trends are established; a few points should be noted, however:

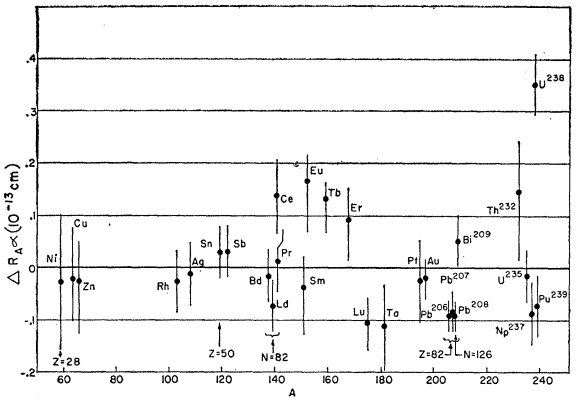

FIG. 23. $\Delta R_{A\alpha}$, the departure of the observed interaction radius from the least squares curve $R_{A\alpha}=(1.414A^{\frac{1}{3}}+2.19)\times10^{-13}$ cm, is plotted against A.

(a) Closed shell effects at $Z=28$, $Z=50$, and $N=82$ are apparently not significant with respect to radius.

(b) The large intrinsic equilibrium quadrupole deformations characteristic of the rare earth region might be expected to result in large interaction radii. Eu, Tb, and Er do indeed appear large, but Lu and Ta, which have very large measured quadrupole moments, appear small. Thus no correlation between radius and quadrupole deformation seems possible in this region.

(c) We feel that the radii for the Pb isotopes are significantly low (about 1%). As can be seen by reference to Table I, a number of measurements at two different angles gave highly consistent results. (For the case where best-fit and crossover radii disagree, Pb^{208} at 42°, the best-fit radius is still lower than the crossover radius.) No difference between isotopes is seen, although the doubly magic Pb^{208} might be expected to be smallest.

(d) The addition of a single proton to $_{82}Pb^{208}$ to make $_{83}Bi^{209}$ results in an increase in radius which is appreciably larger than the internal errors.

(e) Five targets heavier than Bi were studied. $_{92}U^{235}$, $_{93}Np^{237}$, and $_{94}Pu^{239}$ radii fall slightly below the least-squares curve of Eq. (3). $_{90}Th^{232}$ may be significantly high. $_{92}U^{238}$, with $\Delta R_{A\alpha}=+0.35\times10^{-13}$ cm(3.1%), exhibits the greatest departure of all targets observed. Alpha-decay radius determinations[23] also indicate that Th^{232} and U^{238} have large radii, at least when compared with their even-even neighbors.

The large U^{235}-U^{238} difference is of particular interest since proton configurations are, presumably, identical for the two isotopes. As a check on the results obtained for crossover radii, sharp-cutoff cross-section calculations were carried out in detail (Fig. 24). It is seen that the experimental curve for U^{238} is straddled, below the break, by calculated cross sections for $R=11.46$

[21] J. S. Blair (to be published).
[22] G. Igo and R. Thaler, Phys. Rev. **106**, 126 (1957).
[23] I. Perlman and F. Asaro, *Annual Review of Nuclear Science* (Annual Reviews, Inc., Stanford, 1954), Vol. 4, p. 157.

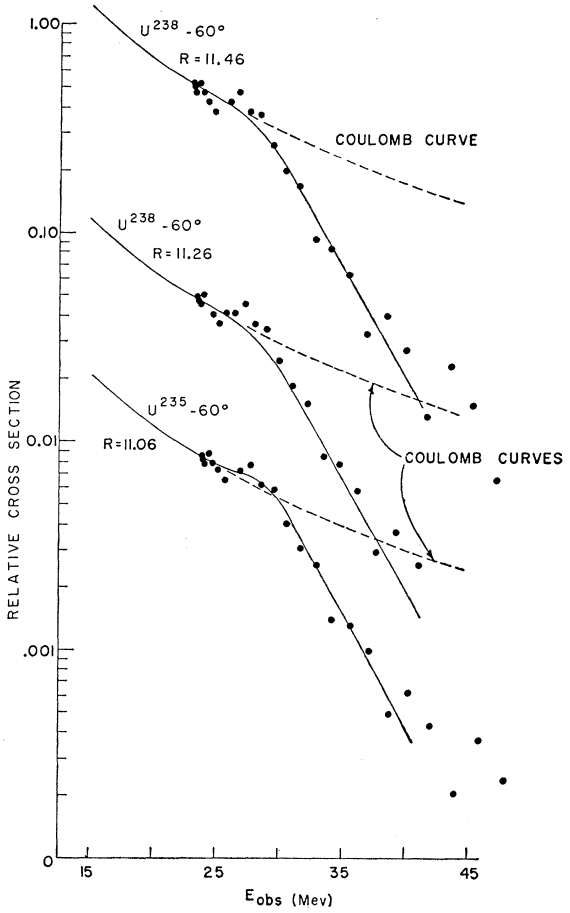

FIG. 24. Cross section *versus* energy for elastic scattering of alpha particles from uranium. The two upper solid curves represent the experimental scattering from U^{238} for laboratory angle $=60°$; the dots are the computed cross sections for $R=11.46$ and 11.26×10^{-13} cm for center-of-mass angle$=60°$. The lowest solid curve represents the experimental scattering from U^{235} for laboratory angle$=60°$, while the dots are computed cross sections for $R=11.06\times10^{-13}$ cm for center-of-mass angle$=60°$.

(10^{-13} cm) and $R=11.26$; if we make the center-of-mass correction discussed earlier, the best-fit radius is consistent with the crossover radius 11.30 ± 0.06. In contrast to this it will be observed that the experimental curve for U^{235} lies close to the calculated points for $R=11.06$; with the same correction, the best-fit radius is in fact compatible with the crossover radius 10.90 ± 0.05. Thus there is little doubt that differences in neutron configuration result in a significantly larger radius for U^{238}.

The over-all results for interaction radii present a picture having a high degree of internal consistency. To compare our results with other nuclear radius determinations, we should include external errors in the calculations. We then find

$$R_{A\alpha}=r_0A^{\frac{1}{3}}+b;\quad r_0=(1.414\pm0.042)\times10^{-13}\text{ cm},\quad b=(2.19\pm0.20)\times10^{-13}\text{ cm}. \quad (3')$$

5. *Comparison with Other Results*

Measurements of nuclear radii depend, of course, not only upon the phenomena under observation but upon the theoretical models in terms of which they are interpreted. Almost without exception, methods dependent upon interactions involving specifically nuclear forces have given values for r_0 ranging from 1.3 to 1.5×10^{-13} cm, whereas those for which only electromagnetic interactions are important have given values between 1.0 and 1.2×10^{-13} cm. The first group[24] includes studies of high-energy neutron scattering, alpha decay, and charged particle reactions. In the second group[24] are studies of mirror nuclei, isotope shift in line spectra, μ-mesic x-rays, and high-energy electron scattering.

If we consider the differences in measurements and models, the large interaction radii obtained from the present experiments are not inconsistent with either the charge distributions resulting from the electromagnetic measurements or the mean radii obtained from optical model analysis of alpha scattering (which are also smaller than the present interaction radii).

From the nuclear potential point of view, the explanation is that the interaction radius is essentially equivalent to the location of the top of the l'th potential barrier; it can be shown that a relatively weak attractive nuclear potential (1–5 Mev) is sufficient to change the sign of the slope of the barrier, so that the barrier summit is located at a distance considerably greater than the usual mean radius. This argument is discussed quantitatively elsewhere.[21]

The interaction radii may be understood in terms of the existing nuclear charge distributions[25–27] if the interaction between alpha and nuclear matter is sufficiently strong to cause a moderate interaction with the nuclear fringe. While the mean electromagnetic radii are small, $(1.07\pm0.02)A^{\frac{1}{3}}\times10^{-13}$ cm, the surface thickness (during which the charge density falls from 0.9 to 0.1 times the central value) is about 2.4×10^{-13} cm. The charge distributions thus have a tail which extends considerably beyond the mean radius; for example, the mean radius for Au is about 6.4×10^{-13} cm, yet at a radial distance of 8.0×10^{-13} cm the charge density is still about 5% of the central value if a Fermi or modified Gaussian distribution is assumed.[25] Further, electron scattering experiments also indicate an appreciable size for the alpha particle; the "rms radius" is 1.6×10^{-13} cm.[27] If in addition one includes a very modest nuclear force range, the present interaction radii then seem plausible without any special assumption that the nuclear distribution is larger than the proton distribution. In fact, the present experiments give indications of

[24] For a more complete discussion see, for example, R. Hofstadter, Revs. Modern Phys. **28**, 214 (1956).
[25] Hahn, Ravenhall, and Hofstadter, Phys. Rev. **101**, 1131 (1956).
[26] Fregeau, Helm, and Hofstadter, Physica **22**, 1195 (1956).
[27] R. W. McAllister and R. Hofstadter, Phys. Rev. **102**, 851 (1956).

TABLE II. Comparison of effective radii[a] from (α,α), (α,α'), and (α,p) reactions and interaction radii $R_{A\alpha}$ from extrapolation of elastic scattering results to low A.

Target	Reaction	Energy of incident alpha (Mev)	Excitation of residual nucleus (Mev)	Type of analysis	Effective radius (10^{-13} cm)	Interaction radius $R_{A\alpha}$ [Eq. (3)] (10^{-13} cm)	Reference
Li^6	α, α'	31.5	2.19	ABM[b]	6.6	4.76	29
Li^6	α, α'	31.5	4.5	ABM	5.8	4.76	29
Be^9	α, α	48	0	Diffraction	4.9	5.13	30
Be^9	α, α'	48	2.43	ABM	5.4		30
Be^9	α, α'	44	2.43	ABM	5.5		31
B^{10}	α, p	4.9–8.1	0	ABM	5.4	5.24	32
C^{12}	α, α'	48	4.43	ABM	5.56	5.43	33
C^{12}	α, α'	31.5	4.43	ABM	5.5		29
C^{12}	α, α'	31.5	7.65	ABM	5.9		29
C^{12}	α, p	41.5	0	ABM-stripping ABM-knockout	5.1 5.75		34
C^{12}	α, p	31	0	ABM-stripping ABM-knockout	6.1 6.6		34
Ne^{20}	α, α	18	0	Diffraction	5.8	6.03	35
Ne^{20}	α, α'	18	1.63	ABM	6.65		35
Mg^{24}	α, α'	48	1.37	ABM	6.6	6.27	33
Mg^{24}	α, α'	42	1.37	ABM	6.54		36
Mg^{24}	α, α'	31.5	1.37	ABM	6.4		29
P^{31}	α, p	7.0, 8.1	0	ABM	6.9	6.63	32
A^{40}	α, α'	18	1.46	ABM	7.12	7.03	35

[a] Probable errors are not given here. Where stated in original references, they range from ± 0.2 to $\pm 0.5 \times 10^{-13}$ cm or more. They are especially large for the lightest elements and for very low incident alpha energy in the heaviest elements.
[b] See reference 28.

sensitivity to slight changes in either neutron or proton configuration, as we have seen in the Pb-Bi comparison above and as we shall note further below (Sec. V). Our large intercept distance b is probably in large part due to the extent of the alpha particle itself.

There is an increasing body of evidence for large interaction radii for alpha-particle reactions in light elements. Interpretation of inelastic alpha-scattering experiments has been made in terms of direct-surface-interaction theories such as that of Austern *et al.*[28] In these interpretations, the observed differential cross sections are expressed as functions of scattering angle in terms of appropriate spherical Bessel functions $j_n(QR)$; Q is the momentum transfer and R is an effective radius for the particular process. Similar analyses have been made of the observed angular distributions of protons from (α,p) reactions in elements ranging from Li to P. Although there is perhaps little reason to expect even approximate agreement between interaction radii calculated by extrapolation of Eq. (3) and the effective radii found for (α,α') and (α,p) reactions in these light elements, the agreement is remarkably close. (Li^6 is an exception.) Table II summarizes the available data.[29–36] Probable errors are not listed, since they are not stated in most of the original references; where they are stated, they range from ± 0.2 to $\pm 0.5 \times 10^{-13}$ cm. The uncertainties are especially large for the lightest elements and for very low incident alpha energy in the heaviest elements.

Agreement of the present data with interaction radii determined by sharp-cutoff analysis of angular distributions of elastically scattered alpha particles is good; this will be discussed elsewhere.[21]

V. THEORY AND RESULTS: FINE STRUCTURE

We have seen (Sec. III) that the experimental curves of cross section *vs* energy are characterized by two features which are distinct from the general trend of Coulomb dependence at low energy and exponential falloff at high energy. First, structure is sometimes apparent in the energy region just before the downward break, usually taking the form of a single region in which the cross section is appreciably above Coulomb. (We have termed this feature the "rise.") Second, diffraction-like oscillations are evident at high energies in some of the curves for the lightest elements among those studied. In the discussion which follows, we shall refer to the rise and the diffraction oscillations as "fine structure."

A. Fine Structure and the Sharp-Cutoff Model

In Sec. IV we showed that both the rise and the diffraction oscillations appear in the results of the sharp-cutoff calculations. We shall now attempt to

[28] Austern, Butler, and McManus, Phys. Rev. **92**, 350 (1953); hereafter referred to as ABM.
[29] H. J. Watters, Phys. Rev. **103**, 1763 (1956).
[30] R. G. Summers-Gill, University of California Radiation Laboratory Report UCRL-3388, 1956 (unpublished).
[31] G. W. Farwell and D. D. Kerlee, Bull. Am. Phys. Soc. Ser. II, **1**, 20 (1956); J. S. Blair and E. M. Henley, Bull. Am. Phys. Soc. Ser. II, **1**, 20 (1956); Progress Report, Cyclotron Research, University of Washington, 1956 (unpublished).
[32] P. von Herrmann and G. F. Pieper, Phys. Rev. **105**, 1556 (1957).
[33] F. J. Vaughn, University of California Radiation Laboratory Report UCRL-3174, 1955 (unpublished).
[34] R. Sherr and M. Rickey, Bull. Am. Phys. Soc. Ser. II, **2**, 29 (1957); M. Rickey (private communication).
[35] Seidlitz, Bleuler, and Tendam, Bull. Am. Phys. Soc. Ser. II, **1**, 29 (1956); L. Seidlitz, Nuclear Physics Progress Report No. 6 (Purdue Research Foundation), U.S.A.E.C. Report COO-173 (1956) (unpublished).
[36] P. C. Gugelot and M. Rickey, Phys. Rev. **101**, 1613 (1956).

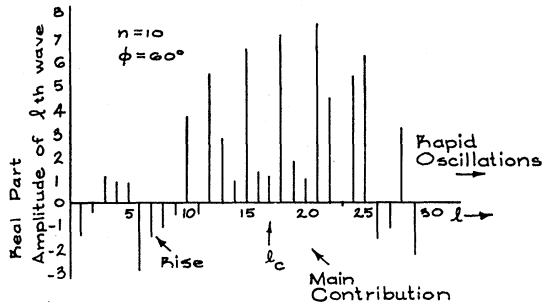

FIG. 25. Real part of the amplitude of the lth outgoing partial wave for pure Coulomb scattering as a function of l for the case $n=10$ and center-of-mass angle $\phi=60°$.

provide more insight on how such fine structure arises as a consequence of the model assumed. In later paragraphs (Sec. VC) we shall see how the structure is likely to be altered in more sophisticated calculations.

In Fig. 25 a typical plot is shown of the real part of the amplitude of the lth outgoing partial wave for pure Coulomb scattering; the particular case $n=10$ and $\phi=60°$ is illustrated. (The argument which follows can be made as easily with the imaginary as with the real part of the amplitude as long as the sum over all partial waves is not close to zero.) Inspection indicates several noteworthy features of this graph: (a) There is a large range in l over which the amplitudes are all of the same sign. The parameter $l_{cl}=n\cot(\phi/2)$, which is the classical angular momentum divided by $\hbar$, lies roughly at the center of this group. Thus in a sense this range of l defines the extent of the "wave packet" in l-space, centered on the classical value of angular momentum which comprises the chief contribution to the pure Coulomb scattering at this angle. (b) Before the coherent positive region there is a smaller negative coherent portion. (c) Superimposed on the general pattern are fluctuations, which occur in this case with a periodicity $\Delta l\sim 3$. (d) As one proceeds beyond the central coherent region the amplitude oscillates around zero with increasing magnitude.

Let us now examine the scattering predicted by the sharp-cutoff model as a function of R with the aid of this diagram and Fig. 3 of reference 3. The scattering amplitude in this model is simply the amplitude for pure Coulomb scattering minus the contributions of all partial waves up through the critical angular momentum defined by Eq. (2). If R is such that all waves are absorbed up to $l'<6$, there is little change from the pure Coulomb cross section since the amplitudes of the absorbed partial waves are small and oscillate in sign. If $l'\sim 10$, the cross section rises, since we have cut out the coherent contribution to the amplitude which is opposite in sign to the main contribution. Since the main "wave packet" is always preceded by a small coherent contribution of opposite sign, the sharp-cutoff model yields an initial rise. As l' increases from ~ 10 to 25, the cross section rapidly drops below the pure Coulomb value; this is because we are eliminating the partial waves which are the chief contributors to pure Coulomb scattering. For R so large that $l'>25$, the cross section oscillates around an average value $\sim(1/10)\sigma_c$; the behavior reflects the fact the central "wave packet" has been subtracted and only the rapid oscillations at the wings of the "wave packet" remain. The diffraction oscillations observed over the entire range of l have the periodicity of the fluctuations in the partial amplitudes for pure Coulomb scattering.

In translating these features into a prediction of cross section *vs* energy, R is fixed while n and the corresponding l' for the given R are varied. The initial rise and the diffraction oscillations survive this procedure. The extent to which each is present depends in a predictable way upon scattering angle and nuclear charge. Because of the sharp-cutoff assumption, both features are intimately related to the nature of the nuclear surface; one might expect surface diffuseness or large departures from sphericity to suppress them strongly. These points will be discussed more fully below (Sec. VC).

B. The Rise: Experimental

The variation of fine structure from one element or nuclide to another manifests itself most sharply in the rise. A semiquantitative study of the rise was made through an "area" parameter S defined by

$$S=\int_{E_1}^{E_2}\left(\frac{\sigma-\sigma_c}{E}\right)dE.$$

$(\sigma-\sigma_c)/\sigma_c$ is the fractional excess of the experimental cross section over the Coulomb cross section, and E_1 and E_2 are the energies which define the extent of the rise.

Plots of S against A are shown in Fig. 26 (42°) and Fig. 27 (60°). The error shown for each point corresponds to the extreme range considered possible for

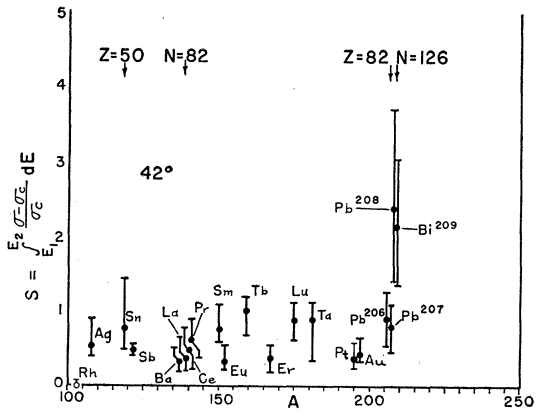

FIG. 26. The parameter S, a measure of the area of the rise in the experimental curve above the Coulomb curve, is plotted against A for the 42° data.

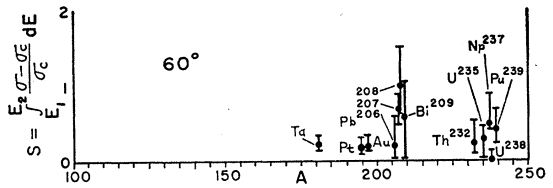

FIG. 27. The area parameter S is plotted against A for the 60° data.

normalization of the experimental curve to the Coulomb curve at low energy; this range is sufficient for large uncertainties in S in many cases. A similar plot of S (60°) against the neutron number N is given in Fig. 28. These three plots represent an attempt to systematize differences and trends which are actually more readily recognized in a qualitative way by reference to the cross section curves (Figs. 1–14).

No estimate of S was made for Ni, Cu, and Zn, since for these elements only a short portion of the Coulomb region was accessible.

The largest rise in the Rh-Ag-Sn-Sb sequence is at Sn ($Z=50$), coinciding with a closed proton shell. Since a natural Sn target was used, averages over the six principal isotopes are represented in the measurements. It would be desirable to investigate separated isotopes of Sn, since it is possible that even greater differences in structure might be observed with single isotopes. The rise is suppressed completely in Rh; in this respect Rh resembles only U^{238} among all other targets investigated.

The Ba-La-Ce-Pr series is especially interesting since these targets have the same (magic) neutron number, 82. We thus observe surface differences which may be attributed solely to proton configuration. The observed trend of increasing rise with increasing Z in this region at 42° does not correspond to the trend in quadrupole moments observed or anticipated on the basis of the shell model.[37] A similar but less well-defined trend is observed at 60°.

In the region Sm to Ta, a general correlation between radius (Fig. 23) and rise (Fig. 26) is noted, with large rise being associated with small radius. Tb is an exception.

The separated isotopes of Pb show outstanding differences in the curve shapes (Figs. 12, 13, 26–28). The largest rise at both 42° and 60° is observed for Pb^{208}. At 42° the singly magic ($Z=82$) Pb^{206} and Pb^{207} exhibit smaller rises which are, however, slightly larger than that observed for the nearby element Au. At 60° a definite trend is observed for the Pb isotopes: the rise increases as N goes from 124 to 125 to the closure at 126. The very large rise at Pb^{208} probably indicates an especially well-defined nuclear boundary for this doubly magic isotope. $_{83}Bi^{209}$, with its single additional proton, is very much like Pb^{208}, though we have seen that it has a larger sharp-cutoff radius.

Th^{232}, U^{235}, Np^{237}, Pu^{239}, and U^{238} were studied at 60° only. In the order listed, they form a series of nuclides increasing in neutron number consecutively by steps of one. The general trend of S with N (Fig. 28) shows a maximum rise for Np^{237} ($N=144$), with smaller values at lower and higher neutron numbers. U^{235} has a moderate rise while U^{238} has zero rise.

A correlation between interaction radius and rise is observed in this region, with large rise (Fig. 28) again corresponding to small radius (Fig. 23). The large differences in U^{235} and U^{238} with respect to both rise and interaction radius support the conjecture that the neutron configuration strongly influences the nature of the nuclear surface.

C. Discussion

Let us first briefly summarize the experimental information concerning the initial rise and diffraction oscillations. (a) In the present experiments an initial rise above Coulomb is observed for most elements investigated; the height and area fluctuate as one moves through the periodic table, with maxima observed at the closing of a nuclear shell; there is some indication that the rise slowly increases with Z. The rise decreases with increasing scattering angle. The rise is absent in scattering from Rh and U^{238}. Angular distributions[4–6] of alphas elastically scattered from heavy elements display a similar rise; measurements with the five targets Ag, Ta, Au, Pb, and Th indicate that the rise increases with increasing Z at constant E. (b) The diffraction oscillations are not observed in the energy dependence of the scattering cross sections for the heavy nuclei. They appear for light nuclei (Al, Zn, Cu) and may be present for some intermediate nuclei (for example Rh and Ag) in the region well below Coulomb. Such oscillations are more prominently displayed in angular distributions; they are apparent, even in the region of the break, when 48-Mev alphas are scattered from the heavy but magic nucleus, Pb (reference 6), and are markedly present for Ag and lighter nuclei, generally increasing in amplitude as Z decreases at constant E or as E increases at fixed Z (references 6, 8–10).

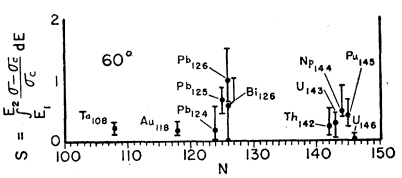

FIG. 28. The area parameter S is plotted against neutron number N for the 60° data on monoisotopic targets.

[37] Way, Kundu, McGinnis, and van Lieshout, *Annual Review of Nuclear Science* (Annual Reviews, Inc., Stanford, 1956), Vol. 6, p. 146.

1. *Effects of Improved Boundary Conditions*

We have seen in detail in Sec. VA above how both the initial rise and the diffraction oscillations appear as consequences of the sharp-cutoff calculations. Some of the features described will be maintained in more sophisticated computations which allow for appreciable nuclear absorption such as those based on the Feshbach-Weisskopf boundary condition[38,39] and the complex nuclear potential.[22,39–43] It has been previously pointed out[3] that the Feshbach-Weisskopf boundary condition leads to the asymptotic values $\eta_l \to 0$ for $l \ll l'$ and $\eta_l \to \exp(2i\sigma_l)$ for $l \gg l'$: what features of the sharp-cutoff calculation are maintained will be a function of how wide in l space is the transition region between these two limiting values of the outgoing amplitude. In particular, it is anticipated that as long as n is large (so that the contribution of each partial wave is small compared to the total Coulomb amplitude), the general trend of the cross section will be unchanged from the sharp-cutoff prediction in the region just below the break; the width of the pure Coulomb "wave packet" is so great that it is not critical whether the transition is sharp or smoothed over many l. On the other hand, the magnitude of the diffraction oscillations and initial rise should depend more subtly on the penetration depth and surface taper; the spacing of the diffraction oscillations, however, should not depend essentially on such details since that reflects the periodicity of the amplitudes for pure Coulomb scattering. Further, there should be a considerable difference in the magnitudes of the cross sections computed with sharp-cutoff and improved boundary condition models when the transition region lies beyond the main contribution to the Coulomb amplitude.[44]

Machine computations with the optical model now being undertaken bear out the remarks of the previous paragraph.[43,22] In particular, Cheston and Glassgold[43] find that for an optical calculation which gives a good fit for the 22-Mev alpha angular distribution from Ag, the transition from pure absorption to pure Coulomb scattering occurs in a band of width $\Delta l \sim 4$. Further, the band is centered about $l'=10$ or 11, which is the cutoff angular momentum giving the best fit of the sharp-cutoff angular model to the data. We present a detailed discussion of the connection between the optical-model parameters and the sharp-cutoff radius elsewhere.[21]

The question now naturally arises: Is it possible to make any further general statements about the fine structure without performing computations based on some more detailed models? We believe that some additional comments within the framework of the sharp-cutoff model are pertinent concerning (a) damping of fine structure as a function of n and angle, and (b) effects due to ellipsoidal distortions of the nuclear surface.

2. *Further Details of Sharp-Cutoff Results*

(*a*) *Damping of fine structure versus n and angle.*— Consider the typical graphs in Fig. 29 of the computed ratio $G \equiv \sigma/\sigma_c$ *versus* l' for several values of n at fixed angle ($\phi=33°$). One notes that: (1) The spacing, Δl, of the rapid oscillations is roughly independent of n and l'; at this angle $\Delta l \sim 5$. (2) The magnitude of the oscillations at corresponding portions of the pattern slowly decreases as the classical parameter n increases. (This reflects the fact that the relative contribution of an individual partial wave decreases as the total Coulomb amplitude becomes larger.) (3) The oscillations are relatively more important when the ratio G is small. (4) The initial rise is somewhat higher for larger n and the "width" of the rise, δl, is roughly linear in n; at 33°, $\delta l \sim (3/4)n$.

It is convenient to relate the spacing Δl to a distance, namely, the difference in the classical turning points between the l'th and $(l'+\Delta l)$th partial waves, which we term ΔR. From Eq. (2) we obtain

$$R = D_{180}\{\tfrac{1}{2}+\tfrac{1}{2}[1+(l'/n)^2+(l'/n)(1/n)]^{\frac{1}{2}}\}, \quad (4)$$

where $D_{180}=ZZ'e^2/E$. From this we find

$$\Delta R = \left(\frac{D_{180}}{2n}\right)\left\{\frac{l'/n}{[1+(l'/n)^2]^{\frac{1}{2}}}\Delta l\right\}, \quad (5)$$

which for large (l'/n) becomes

$$\Delta R \cong \lambda\!\!\!^{-}\Delta l. \quad (6)$$

We shall be guided by the intuitive notion that when ΔR is small compared to some distance characteristic of the surface fuzziness, the oscillations are easily damped; when ΔR is large, we assume the converse. In similar fashion one can introduce a thickness, δR, corresponding to δl.

Let us now examine the implications of these observations for scattering from two nuclei of different charge, $Z_1 > Z_2$, at the same value of G. In the region just past the break, it is a good approximation to relate

[38] H. Feshbach and V. F. Weisskopf, Phys. Rev. **76**, 1550 (1949).
[39] N. Oda and K. Harada, Progr. Theoret. Phys. (Japan) **15**, 545 (1956).
[40] C. B. O. Mohr and B. A. Robson, Proc. Phys. Soc. (London) **A69**, 365 (1956).
[41] W. B. Cheston and A. E. Glassgold, Bull. Am. Phys. Soc. Ser. II, **1**, 339 (1956).
[42] Igo, Thaler, and Hill, Bull. Am. Phys. Soc. Ser. II, **1**, 384 (1956).
[43] W. B. Cheston and A. E. Glassgold, Phys. Rev. **106**, 1215 (1957).
[44] It is relevant here to comment on the fuzzy modification of the sharp-cutoff model proposed by Wall, Rees, and Ford[4] and by Ellis and Schechter[6] in discussing angular distributions. The transition region is explicitly introduced through a weight factor, W_l, which multiplies the pure Coulomb amplitude and varies from 0 to 1 over a range of l near l'. The fact that these recipes prove incapable of completely damping out the fine structure should not be interpreted as an argument against the existence of a transition region; the weight factor is in general a complex number and it does not follow that the real linear weight factors used by these authors necessarily simulate an optical-model calculation.

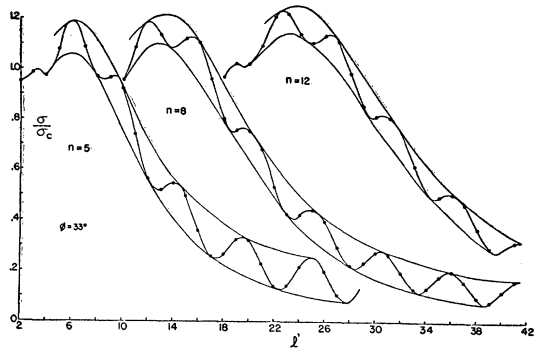

FIG. 29. Computed σ/σ_c *versus* l' for $n=12$, 8, and 5 at center-of-mass angle $\phi=33°$. The dots are the computed values which are then joined by the interpolated solid curve. The envelopes of these curves are also indicated by solid lines.

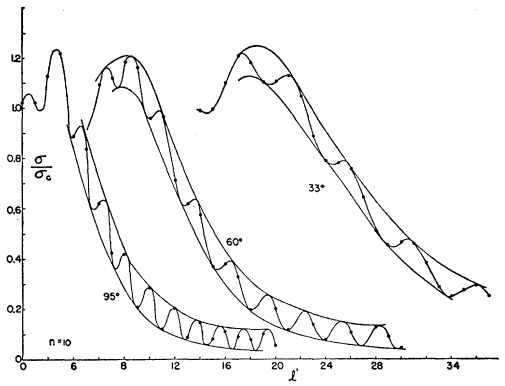

FIG. 30. Computed σ/σ_c *versus* l' for center-of-mass angles $\phi=33°$, 60°, and 95° when $n=10$. The dots are the computed values which are then joined by the interpolated solid curve. The envelopes of these curves are also indicated by solid lines.

the energies at the same value of G, E_1 and E_2, to the charge through

$$(R_1/R_2)\cong(D_{180,1}/D_{180,2}), \tag{7}$$

so that

$$(E_1/E_2)\cong(Z_1/Z_2)^{\frac{2}{3}}. \tag{8}$$

Thus

$$(n_1/n_2)\cong(Z_1/Z_2)^{\frac{2}{3}} \tag{9}$$

and

$$(\Delta R_1/\Delta R_2)\cong(Z_2/Z_1)^{\frac{1}{3}}. \tag{10}$$

It is consequently easier to damp the rapid oscillations of nucleus 1 at the same value of G because (1) with $n_1>n_2$ the magnitude of oscillations is smaller and (2) the same thickness of surface fuzziness will produce greater damping in 1 than in 2.

On the other hand, if surface conditions are comparable, the initial rise should be more pronounced for the nucleus with larger charge; this is because the maximum of the mean height is somewhat larger for greater n, and the ratio of effective thicknesses associated with the width of the rise varies as

$$(\delta R_1/\delta R_2)\cong(Z_1/Z_2)^{\frac{1}{3}}. \tag{11}$$

Let us next consider the computed G *versus* l' for fixed $n(n=10)$ at several angles, as illustrated in Fig. 30. It is seen that: (1) the spacing, Δl, decreases markedly as ϕ increases: $\Delta l\sim5$, 3, and 1.8 at $\phi=33°$, 60°, and 95°, respectively; (2) the width of the rise, δl, is also a strong function of angle: $\delta l\sim7.5$, 4, and 2 at 33°, 60°, and 95°, respectively; (3) the magnitude of the oscillations and the height of the rise do not appreciably change with angle.

Statement (2) explains why the rise is more pronounced for the same element as the angle is decreased: the increase in δR due to the smaller angle overcomes the decrease resulting from the slightly smaller value of n and wavelength at the new (higher) energy of the rise.

Consideration of Figs. 29 and 30 also makes it possible to understand qualitatively the observation of Igo, Wegner, and Eisberg that the diffraction structure in angular distributions from the same target is more pronounced as the energy is increased; this feature is illustrated in Figs. 13 and 14 of reference 10. For higher energy at the same value of G, the magnitude of the oscillations is greater for the smaller n and ΔR is larger at the smaller angle in spite of the diminished wavelength. The same argument indicates why Ellis and Schechter[6] find oscillations in the angular distributions of 48-Mev alphas scattered from Pb and Ag, while the oscillations either are absent or occur in the region well below Coulomb in the present and previous experiments at fixed angle.[2] It is for this reason that we feel justified in averaging over the diffraction oscillations in the process of obtaining the crossover radii.

Further, the fact that the rise at fixed energy generally increases with Z (references 4–6) is understandable since the mean maximum height increases with n, and $\delta l\propto n$, at fixed angle; as Z increases, the rise actually moves backward in angle but the shift is not enough to cause δR to decrease.

(*b*) *Damping effect of ellipsoidal deformation.*—The effects of one damping mechanism—namely, ellipsoidal distortion of the nuclear surface—can be quantitatively estimated with the sharp-cutoff model. A detailed discussion of scattering from distorted nuclei will be presented elsewhere[45]; only some summary comments are made here.

Using the impulse approximation, justified when the nuclear collision time is short compared to the period for nuclear rotation, and neglecting effects due to the electric quadrupole moment (a nontrivial assumption), Drozdov[46] has derived expressions for cross sections into the various nuclear rotational states in terms of the scattering amplitudes from stationary ellipsoidal nuclei suitably averaged over possible orientations. In particular, the "elastic" cross section summed over all final rotational states and averaged over initial states is

[45] J. S. Blair and F. G. Major, Bull. Am. Phys. Soc. Ser. II, **1**, 336 (1956).

[46] S. I. Drozdov, J. Exptl. Theoret. Phys. U.S.S.R. **28**, 734, 736 (1955) [translation: Soviet Phys. JETP **1**, 588, 591 (1955)].

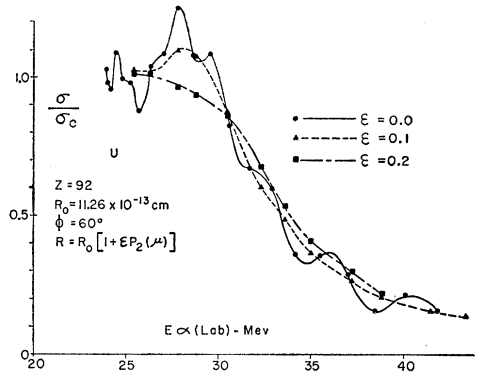

FIG. 31. Computed σ/σ_c *versus* energy for alpha particles scattered from U^{238} at center-of-mass angle $\phi=60°$, summed over nuclear rotational states for $R_0=11.26\times10^{-13}$ cm and $\epsilon=0$, 0.10, and 0.20. The sharp-cutoff radius R is assumed to have the form $R=R_0[1+\epsilon P_2(\cos\theta)]$, where θ is the angle between the principal axis of the nucleus and the axis of symmetry for a classical Coulomb trajectory.

simply the average over all orientations of the cross section for a classically oriented nucleus.

The sharp-cutoff model is particularly amenable to the above treatment when the nuclear orientation θ and the deformation ϵ are assumed to be simply related to the only nuclear parameter in the model, the cutoff radius R, by $R=R_0[1+\epsilon P_2(\cos\theta)]$, where θ is the angle between the principal axis of the nucleus and the axis of symmetry for a classical Coulomb trajectory.

The ratio of "elastic" to Coulomb cross section for U^{238} at 60° is plotted *versus* E in Fig. 31 for three values of ϵ: $\epsilon=0$, 0.10, and 0.20. The transition rate to the first excited state of U^{238} by Coulomb excitation[47] yields $\epsilon\sim0.26$. An ellipticity of 0.10 appears ample to damp the rapid oscillations, and one as large as 0.20 suffices to remove the initial rise (as is indeed observed) and to displace the pattern toward higher energies.

It is tempting to regard such distortions as the prime cause for damping of the initial rise, but the following observations make it likely that it is only one of several contributing mechanisms: (1) The measured ellipticity of Th is roughly the same as that of U^{238}, yet the rise in Th and other neighbors of U^{238} is appreciable. (2) The initial rises in rare earth elements do not correlate well with known ellipticities. A calculation similar to that carried out for U has been performed for Ta; the computed damping is larger than that observed.[48] (3) The striking variations in the rise observed near a closed shell suggest that the role of the surface nucleons is at least as important as that of the collective surface distortion in determining the extent of the rise.

VI. CONCLUSIONS

The sharp-cutoff analysis of the energy dependence of alpha-particle elastic scattering cross sections gives a remarkably consistent picture of alpha-nucleus interaction radii for a very wide range of elements. Qualitative features of experimental curves of both cross section *versus* energy and cross section *versus* angle can be accounted for in terms of the sharp-cutoff model. The present experiments exhibit a high degree of sensitivity to the properties of the nuclear surface, and indicate that both proton and neutron configurations have an important influence upon the interaction of an alpha particle with the fringes of the nuclear matter. There is no clear correlation between quadrupole deformations and the experimental results, although such deformations are undoubtedly responsible for some damping of the fine structure of the curves. A number of regions of the periodic table would be worth further exploration, particularly those near closed shells where the effects of changes in neutron or proton configuration might be especially large and subject to nearly independent investigation.

VII. ACKNOWLEDGMENTS

It is a pleasure to thank the following individuals and groups for their special assistance in making this work possible: Professor Ted Morgan and the University of Washington Cyclotron staff for many days of stable cyclotron operation; Mr. Paul Robison for his skillful help in preparing self-supporting target foils and for his assistance with the computations; Mr. Gail Shook and Mr. John Hopkins for valuable help in construction of the proportional-counter telescope; the Machine Accounting Office of the University of Washington for use of the IBM 604 electronic calculator, and Dr. D. Newton of the International Business Machine Corporation for his aid in preparing the code; Mr. F. G. Major and Mr. P. Stevens, who assisted with the computations; Dr. G. Igo, Dr. D. Hill, Dr. W. B. Cheston, and Dr. A. E. Glassgold for stimulating discussion and correspondence and for making available their results prior to publication.

[47] N. P. Heydenburg and G. M. Temmer, *Annual Review of Nuclear Science* (Annual Reviews, Inc., Stanford, 1956), Vol. 6, p. 77, Fig. 10.

[48] The favorable rotational level structure of Ta [F. Boehm and P. Marmier, Phys. Rev. **103**, 342 (1956)] and the fairly large rise observed for Ta at 42° suggested a test of the sensitivity of the experimental results to the admission of alphas scattered with excitation of Ta to low-lying levels. Under normal operating conditions, the 0.136-Mev (first excited) state was partially excluded and higher states were effectively ruled out. The energy acceptance band of the detector was approximately doubled so that the 0.136-Mev state was admitted almost completely and the next two levels (0.303 and 0.482 Mev) were admitted to a considerable degree. No discernible change in the shape or location of the experimental curve resulted.